

Nonlinear heat transfer processes in a two-phase thermofluidic oscillator



Christos N. Markides^{a,*}, Adebayo Osuolale^a, Roochi Solanki^a, Guy-Bart V. Stan^b

^a Department of Chemical Engineering, Imperial College London, London SW7 2AZ, UK

^b Department of Bioengineering and Centre for Synthetic Biology and Innovation, Imperial College London, London SW7 2AZ, UK

HIGHLIGHTS

- ▶ We develop a nonlinear model for a two-phase heat-powered thermofluidic engine.
- ▶ We compare the results with an existing linear model and experimental observations.
- ▶ The two models predict a similar oscillation frequency for the fluid pumping device.
- ▶ The predicted efficiencies are dissimilar and in some cases have different trends.
- ▶ The nonlinear model gives more realistic predictions of actual engine performance.

ARTICLE INFO

Article history:

Received 28 February 2012

Received in revised form 17 September 2012

Accepted 22 November 2012

Keywords:

Thermofluidic oscillator
Low-grade heat
Oscillatory
Heat engine
Nonlinear
Efficiency

ABSTRACT

A two-phase thermofluidic oscillator was recently reported as being capable of undergoing sustained operation when a constant and low temperature difference is applied to the device, which consists of a network of tubes, compartments and two heat exchanger blocks. Within this arrangement a working fluid undergoes thermodynamic property oscillations that describe a heat engine cycle. Previous attempts to model the dynamic behaviour of this thermofluidic engine for performance predictions have been based on linear analyses. These have provided us with useful knowledge of the necessary minimum temperature difference for operation, and the resulting oscillation frequency and efficiency. However, experimental observations suggest a limit cycle operation associated exclusively with nonlinear systems. The present paper presents an effort to devise a nonlinear model for the device. Indicative results from this model are discussed, and the predictions are compared to those from the linear equivalents and experimental observations. The results reveal that although both linear and nonlinear models predict similar oscillation frequencies, the nonlinear model predicts lower exergetic efficiencies. This probably arises from the inability of the linear representation in the thermal domain to capture the saturation in the rate of heat exchange between the working fluid and the heat exchangers. The present effort aims to provide a better understanding of this device and to suggest improved design guidelines for increased efficiency and power density.

Crown Copyright © 2012 Published by Elsevier Ltd. All rights reserved.

1. Introduction

The overwhelming use of fossil fuel combustion for the provision of heat and power, and consequently, the release of the product gases into the atmosphere are issues of growing concern. On one hand these primary energy sources are finite, while the global demand for heat (and/or cooling) and power is increasing. Sustainable and secure energy solutions require a more diverse source base that can be relied on in the longer term. At the same time the potential consequences of the release of combustion gases into the atmosphere to human health and the environment are of crucial interest. In lieu of this, there is an urgent need to seek and to develop alternative sources of energy for heating and power,

including renewable energy sources such as geothermal and solar heat. In addition, there is an important and increasing drive to maximise the overall efficiency of plants and processes in the industrial, transport, residential and public sectors that consume fossil fuels for their operation, via the recovery and re-utilisation of waste heat [1].

Low-grade (that is, low temperature) heat is a classification for sources of heat that are, typically, at 250 °C and below [2]. This class of heat sources includes waste heat from industrial processes, heat from non-concentrated solar thermal collectors and low temperature geothermal water and steam. Low-grade heat is abundantly available, however, its use can often be unfavourable as a consequence of the inherently low thermal efficiencies that can be achieved from its use; a thermodynamic limitation imposed by the second law, and indicated by the low associated Carnot efficiencies.

* Corresponding author. Tel.: +44 (0)20 759 41601.

E-mail address: c.markides@imperial.ac.uk (C.N. Markides).

| | | | |
|----------|--|----------|--|
| σ | real part of a pole | ψ | saturation pressure (maximum pressure fluctuation amplitude), Pa |
| τ | scaling parameter for time, s | ω | angular frequency, rad/s |
| χ | parameter that depends on spatial gradient of the heat exchanger wall temperature at equilibrium, 1/Pa | | |

Thermofluidic oscillators are a class of unsteady heat engines that are capable of utilising low-grade heat to produce an oscillatory motion, and therefore a useful work output. The Non-Inertive-Feedback Thermofluidic Engine (NIFTE), whose output is hydraulic work (i.e., fluid pumping, circulation or pressurisation), is an example of such devices [3–5]. An experimental prototype of the NIFTE has been reported as being capable of operating when placed in-between a hot source and a cold sink with a temperature difference of as low as 30 °C [6]. This prototype, whose key advantages are its simple construction and small number of moving parts, is currently being used as a basis for the development of a low-cost pulsating fluid pump that would convert low-grade heat

(such as solar heat from collectors, or waste heat) to hydraulic work. If the development of this pumping device is successful, it will constitute the first example of a two-phase thermofluidic oscillator ever to be applied practically for energy/carbon savings, and also humanitarian applications for clean water provision.

As shown in Fig. 1a, the NIFTE is also a *two-phase* engine, whose working fluid exists simultaneously in both the vapour and the liquid phases. The cyclic (periodic) evaporation and condensation of the working fluid contained in the device induces a sustained oscillatory fluid motion from stationary (steady) heat sources and sinks, via a hot heat exchanger that interfaces with the heat source and a cold heat exchanger that interfaces with the heat sink.

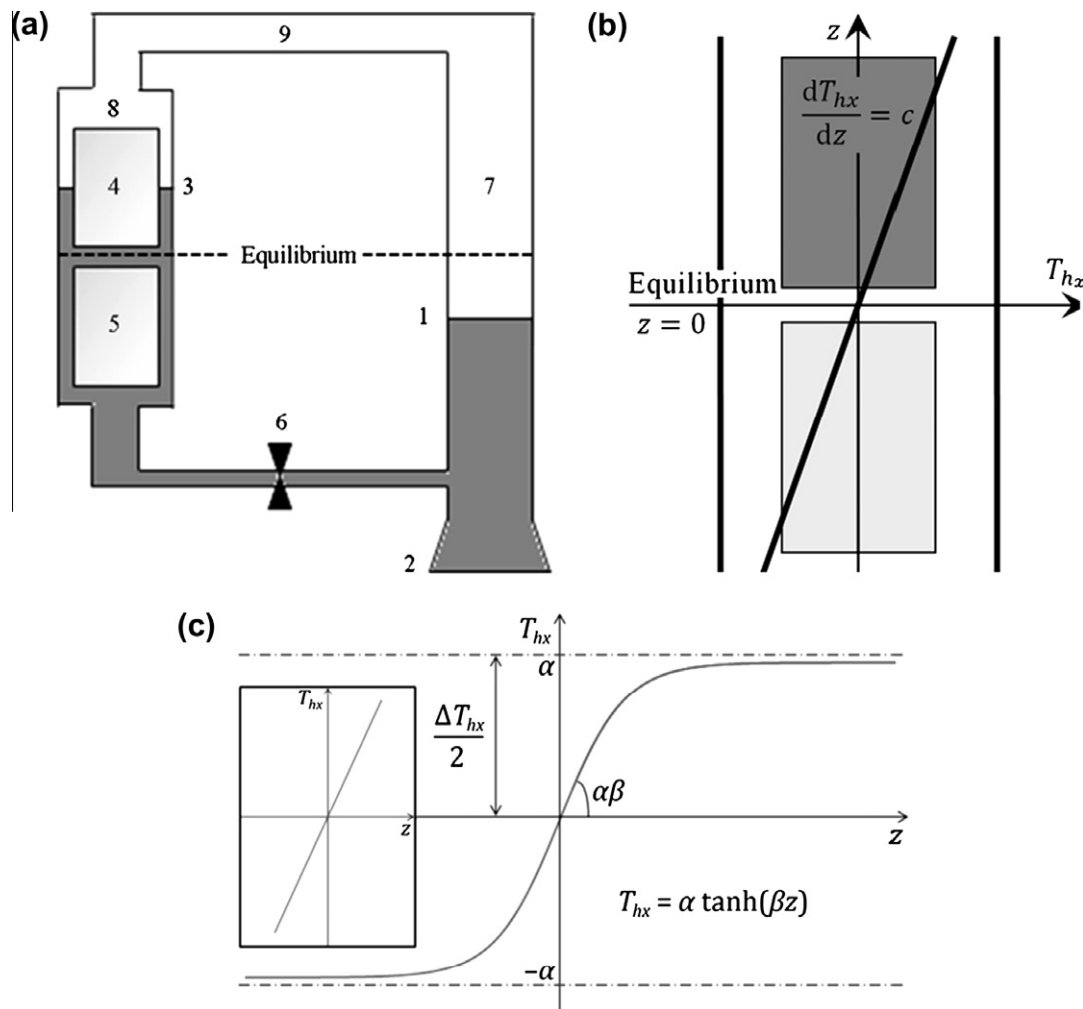


Fig. 1. (a) NIFTE fluid pump schematic. Points 1–9 denote the liquid level in the power cylinder (1), the point of attachment of the load (2), the liquid level in the displacer cylinder (3), the hot heat exchanger (4), the cold heat exchanger (5), the feedback valve in the feedback line (connection) (6), the power cylinder (7), the displacer cylinder (8) and the adiabatic vapour region (9), respectively. (b) Profile of the heat exchanger wall temperature according to the Linear Temperature Profile (LTP) model, superimposed over the heat exchanger blocks within the displacer cylinder walls. The origin corresponds to the state in which the system is at equilibrium, that is when $z = 0$ and $T_{hx} = T_0$. The half-line defined by the LTP model for $z > 0$ corresponds to the HHX temperature profile as a function of displacement from the equilibrium ($z = 0$), whereas that defined for $z < 0$ corresponds to the CHX temperature profile; where HHX denotes the hot heat exchanger and CHX the cold heat exchanger. (c) Nonlinear static relationship between the temperature of the heat exchanger wall T_{hx} and the height of the liquid level in the displacer cylinder z . Here, α is the temperature amplitude and β is a parameter that depends on the slope of around the origin. At the equilibrium position, $z = 0$, the wall temperature is the same as the saturation temperature of the working fluid, which is the equilibrium temperature T_0 . Inset shows the equivalent linear (LTP) profile, with the same gradient at the origin.

In common with other thermofluidic oscillators, the NIFTE depends by design on the establishment of persistent dynamic oscillations to operate. In order to understand the dynamics of the NIFTE, various linear system models have been proposed [3–9]. These models were developed using methods similar to those adopted in earlier studies, such as by Backhaus and Swift [10] for the analysis and development of thermoacoustic engines, but also by Ceperley [11] and Huang and Chuang [12], which exploit the dynamic similarities between the linearised first-order thermal, fluid and thermodynamic processes occurring in the systems under investigation and analogue electronic components. This realisation leads to the development of equivalent electronic oscillator circuits that allow the relatively straightforward prediction of approximate stability/instability¹ criteria and the estimation of heat and work flows, and efficiencies. The knowledge gained by these methods is crucial in the early-stage design of these technologies, when rapid progress is required at short time-scales and with little effort, by concentrating on the dominant underlying processes and effects.

Specifically, the aforementioned approach establishes suitable electrical analogies to the linear first-order spatially lumped thermal-fluid processes in a physical device, which are then represented by passive electrical components. Viscous and pressure fluid flow drag, as well as heat transfer (thermal resistance) are modelled by resistors, hydrostatic pressure and vapour compressibility are modelled by capacitors, and the inertia of the fluid flows (in the liquid state only) in various components is modelled by inductors. The various electrical components are then connected according to the interactions of the thermal-fluid processes in the device, thus giving rise to an electrical oscillator circuit. In order to model the NIFTE, the above mentioned modelling approach was extended by including a description of exergy (or availability) flows, and by allowing for the exergy losses that occur due to the irreversible heat transfer across the finite temperature difference between the external heat source/sink and the working fluid [3–5]. Further information on how the linear network NIFTE models were developed can be found in Refs. [3–9], where the above procedure is described in detail.

The first linear model developed for the NIFTE [3–5] did not include fluid flow inertia, as it was claimed that the NIFTE does not rely on this effect for its operation [2]. However, some degree of inertia will be present inevitably in any physical manifestation of this two-phase engine, owing to the presence of liquid in certain components (the pressure and displacer cylinders, feedback connection and load; see Fig. 1a). The revised ‘inertive’ linear model of the NIFTE proposed in Refs. [6,7] demonstrated that the inclusion of this effect gives more realistic engine predictions than the original ‘non-inertive’ model. As a result of this finding, subsequent models [8,9] have included liquid inertia in their formulation, however, all previous NIFTE models are based on *linearised* descriptions.

Furthermore, by employing the revised non-inertive linear NIFTE model and performing a sensitivity analysis, Markides and Smith [6] proceeded to identify the four most important components that determine the performance of the NIFTE, namely: (i) the feedback connection; (ii) the power cylinder; (iii) the adiabatic volume; and (iv) the thermal resistance associated with the two-phase heat transfer in the heat exchangers. The authors suggested that these components must be designed carefully in order to improve the NIFTE’s performance.

Nevertheless, one key feature of the NIFTE pumping device is that it exhibits *sustained, robust* periodic oscillations, with a specific characteristic amplitude and frequency that neither grow

nor decay during steady-state² operation, when a constant and low temperature difference is applied to the heat exchangers of the device. This behaviour persists despite recognised (though unintended) fluctuations in the temperatures of the hot and cold heat exchangers, and other inevitable natural disturbances to the operation of the device. This can be readily described as an ‘asymptotically stable limit cycle’ behaviour, a characteristic specific to *nonlinear* dynamical systems. As mentioned previously, all models for the NIFTE that have been developed thus far are linear. Although extremely useful in providing some local stability information and some insight into the actual operation and performance of the device, the linear models have noteworthy limitations with regards to their ability to predict reliably the behaviour of what is, actually, a nonlinear system.

The dynamical effects of nonlinearities on the mechanical and thermodynamical characteristics of engines (e.g., efficiency, transient and steady-state behaviours, robustness to physical parameter uncertainties and to *external perturbations*) have been investigated in previous work (e.g., [13–16]). These studies have shown how simple differential equation models that acknowledge the presence of core nonlinear physical elements inherent to these engines can help in understanding their observed nonlinear behaviour, in performing in-depth analyses of their predicted efficiencies, robustness and performance, and in suggesting design solutions that improve their operational characteristics (e.g., engine efficiency and power density). Such models enable the efficient use of the engineering design cycle by allowing *in silico* prediction, analysis and testing of various modifications before actual prototype-testing and implementation. Following the same line of thought, in this paper, we propose, for the first time, a nonlinear Ordinary Differential Equation (ODE) model that takes into account one of the core nonlinear element in a two-phase thermofluidic oscillator, i.e., the inherent physical saturation in the rate of heat exchange between the working fluid and the heat exchangers.

In summary, a more realistic representation of the NIFTE must involve the development of a *nonlinear inertive* model. In the present paper we include a nonlinear element in the description of the device; specifically, we impose a nonlinear description of the two phase heat exchange process that occurs between the working fluid and the engine’s heat exchangers. This model comprises a *modified* static temperature profile imposed on heat exchanger walls, based on an extension of the ‘Linear Temperature Profile’ (LTP) models presented by Markides and Smith [6] and Solanki et al. [7,8]. The resulting ‘Nonlinear Temperature Profile’ (NTP) model is then probed to reveal information about the NIFTE technology.

To this end we perform a dynamical systems analysis³ of the proposed nonlinear inertive model of the NIFTE. This leads to the identification of a key parameter (termed the ‘nonlinear gain’ of the system) through which the emergence of asymptotically stable limit cycle oscillations can be explained and tuned. The approach allows a systematic understanding of the effects of various important parameters on the behaviour and performance (such as the oscillation frequency and amplitude, and the resulting exergetic efficiency) of the model. In a wider context, this nonlinear extension to the linear NIFTE models is expected to allow for much improved predictability, which is crucial for the employment of these models as useful tools in the early-stage engineering design and development of this, and also of other similar technologies.

Proceeding further, we use the results of the present analysis to show how the main characteristics (frequency and amplitude) of the sustained oscillations in the NIFTE, can be adjusted by modifying the physical parameters of the device. This provides us with rigorous information for the design or modification of the NIFTE

¹ Note that the NIFTE operation requires a lack of stability in order to sustain the oscillations.

² By ‘steady-state’ we mean at long times from start-up, after any initial transients have decayed.

³ Specifically, a local stability analysis combined with a bifurcation analysis, and a time behaviour analysis through the numerical integration of the model equations (these are explained in Section 4).

with *a priori* defined engineering specifications such as output flow-rate amplitude and frequency, and efficiency. Finally, the predictions of the nonlinear inertive model are also compared to similar indications that arose from the equivalent inertive LTP models [6–8].

2. Methodology

2.1. NIFTE configuration and operation

Fig. 1a shows a schematic diagram of the NIFTE when it is employed as a fluid (liquid) pump. A full description of the NIFTE pump along with details concerning its operation can be found in any of the Refs. [3–9]. Briefly and referring to Fig. 1a, the vertical tubes denoted by Points 7 and 8 are the power cylinder and the displacer cylinder, respectively. The two cylinders are connected at the top by the vapour tube (9), and at the bottom by the feedback tube and valve (6). Inside the displacer cylinder are the hot (4) and cold (5) heat exchanger blocks, which are the driving components of the device. The NIFTE is filled with a working fluid that exists (simultaneously) both in the liquid (grey region in Fig. 1a) and vapour phases (white region). The hot heat exchanger (HHX) is where heat is taken from an external heat source and supplied to the working fluid causing it to evaporate. Conversely, the cold heat exchanger (CHX) is where heat is rejected from the working fluid causing it to condense. Finally, Point 2 is the NIFTE's connection point with the load. When the NIFTE is used as a pump, this is the point where the device is connected to the liquid medium that is being pumped.

Sustained oscillations are achieved in the NIFTE by the periodic evaporation and condensation of the working fluid (*n*-pentane [5]) in the displacer cylinder (Point 8), which occurs as the vapour–liquid interface level (3) oscillates vertically between the (aluminium [3,5]) HHX and CHX blocks. During the heat addition (evaporation) stage, the working fluid in the liquid phase comes into contact with the HHX in the vertical displacer cylinder (8), which causes it to evaporate. This leads to the generation of vapour in the displacer cylinder, and hence in the combined vapour volume at the top of the device (white region in Fig. 1a). The increase in pressure within the vapour volume as a result of the vapour generation leads to the downward displacement stroke of the vapour–liquid interface level (liquid piston) in the power cylinder (1). As this process takes place the hydrostatic pressure difference between the displacer and power cylinders (which are connected by the feedback line) first decelerates and then reverses the liquid piston flow in the power cylinder, while also causing the liquid level height in the displacer cylinder (3) to drop. Eventually the vapour–liquid interface level in the displacer cylinder comes into contact with the CHX, leading to condensation of the working fluid in the vapour phase over the cold, uncovered CHX surfaces. During the ensuing heat rejection (condensation) process, the reduced pressure in the vapour volume at the top of the device leads to an upward displacement stroke of the vapour–liquid interface in the power cylinder and a rise in the liquid level height in the displacer cylinder (3), until eventually the vapour–liquid interface level in the displacer cylinder comes into contact with the HHX. This completes a cycle of oscillation.

2.2. NIFTE model development

As can be seen in Fig. 1a, two regions can be identified in the NIFTE: (i) a fluid domain where pressure differences (analogous to voltage/potential differences) drive volumetric flow-rates (analogous to currents); and (ii) a thermal domain where the temperature difference (analogous to a voltage/potential difference)

between the heat exchangers and the working fluid drives a heat flow (analogous to current). The following two sections address the modelling of each of these domains.

2.2.1. Fluid domain

The methods adopted by Backhaus and Swift [10], Ceperley [11], Huang and Chuang [12], and later Smith [3–5], are used in the modelling of the fluid domain. The drag experienced by the liquid flows in the load (2) and in the feedback connection (6) are modelled by the inclusion of resistors R (Eq. (1)), while the inertia of the liquid flows in the load, the feedback line, the power cylinder and the displacer cylinder are modelled by inductors L (Eq. (2)). In addition, the hydrostatic pressures in the power (7) and displacer (8) cylinders, as well as the expansion/compression of the vapour volume at the top of the engine (9) are modelled by capacitors C (Eq. (3)). It is assumed that the vapour expansion and compression is adiabatic and reversible, and thus isentropic.

An extensive presentation of the modelling approach that allows the aforementioned electrical analogies to be made can be found in Refs. [6–9]. In summary, for each *dominant* fluid flow or thermodynamic process or effect described above (i.e., drag, inertia, gravity or compressibility) within each major component of the physical device (i.e., load, feedback connection, power cylinder, displacer cylinder, vapour volume), a linearised and spatially lumped first-order governing equation is written in the Laplace domain in the form $U_i = \Delta P_i/Z_i$, where U_i is the (Laplace transform of the) volumetric fluid flow-rate through a particular physical component ' i ' and ΔP_i is the (Laplace transform of the) pressure difference across that component. These equations are analogous to the governing equations of passive electrical components, where Z_i is the impedance of each component.

Now, since the equations describing each process or effect $U_i = \Delta P_i/Z_i$ are linear, the principle of superposition can be applied to account for more than one process or effect within a particular component in the physical device. Thus, working in the Laplace domain, whereby s is the Laplace variable that arises from differentiation in the time domain, the five major NIFTE fluid components can be described in terms of the three types of impedances (R , L or C), as: $Z_{ad} = 1/sC_{ad}$ for the adiabatic vapour volume, $Z_d = sL_d + 1/sC_d$ for the displacer cylinder, $Z_f = R_f + sL_f$ for the feedback connection, $Z_l = R_l + sL_l$ for the load, and $Z_p = sL_p + 1/sC_p$ for the power cylinder. The definitions of the fluid domain electrical parameters R_i , L_i and C_i that result from the analogies and that appear in each impedance Z_i are given below, with respect to physical and geometrical NIFTE variables [6–9]:

$$R_f = \frac{\mu_l l_f}{\pi d_f^4}; \quad R_l = \frac{\mu_w l_l}{\pi d_l^4} \quad (1)$$

$$L_d = \frac{\rho_l l_d}{A_d}; \quad L_f = \frac{\rho_l l_f}{A_f}; \quad L_l = \frac{\rho_w l_l}{A_l}; \quad L_p = \frac{\rho_l l_p}{A_p} \quad (2)$$

$$C_{ad} = \frac{V_o}{\gamma P_o}; \quad C_d = \frac{A_d}{\rho_l g}; \quad C_p = \frac{A_p}{\rho_l g} \quad (3)$$

These parameters are then connected to form the *fluid part* of the electrical network circuit for the NIFTE [6–9], and are also used in the present work to model the same domain (Fig. 2).

Note that, in common with all previous models of the NIFTE, the time-varying fluid flow, heat transfer and thermodynamic property variables are purely oscillatory around their equilibrium values (which coincides with their time-averages) and by convention we are interested only in the magnitude of the fluctuating part of these signals, i.e., $x'(t) = x(t) - \bar{x}$, where $\bar{x} = x_o$ is the time-average (equilibrium) of variable $x(t)$. By definition, the fluctuating parts of all resulting variables $x'(t)$ have a zero mean, and so for simplicity

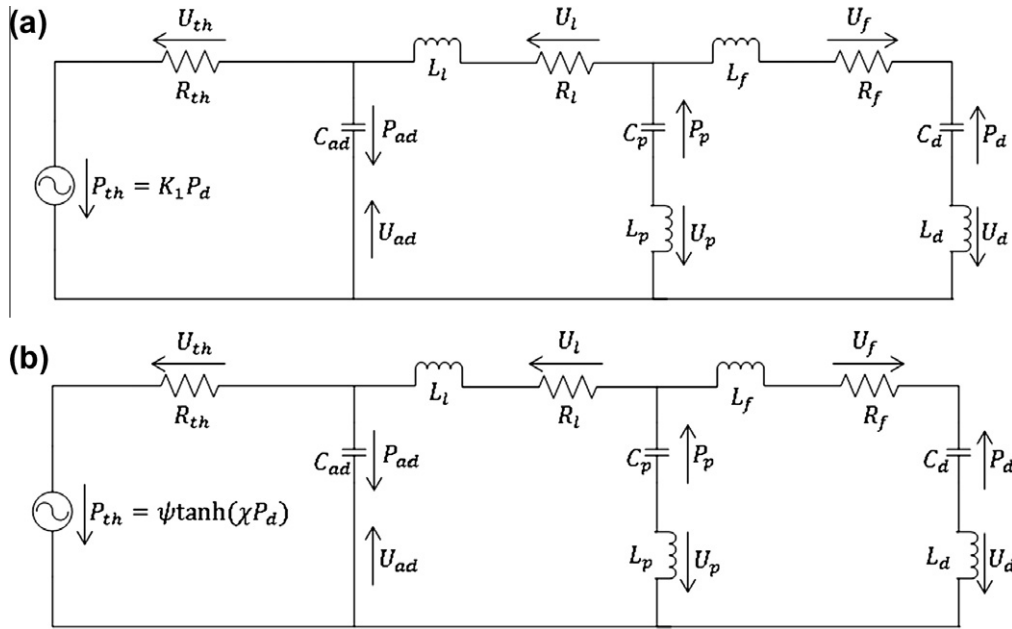


Fig. 2. The complete inertive NIFTE-LTP circuit, as per Refs. [6–8], and the electrical circuit representation of the inertive NIFTE-NTP. Here, ψ is the maximum deviation of the referred pressure from its equilibrium value and χ is a parameter that depends on the slope of the sigmoidal function $\tanh(\cdot)$ around the origin. Further, R_i denotes a resistance, C_i a capacitance, L_i an inductance, P_i a pressure and U_i a volumetric flow-rate. The subscript ‘th’ denotes the thermal domain, ‘ad’ the adiabatic domain, ‘l’ the load, ‘p’ the power cylinder, ‘d’ the displacer (heat exchanger) cylinder, and ‘f’ the combined effect of the feedback line (pipe) and valve.

the primes (\cdot) are dropped from the notation employed throughout this paper. Thus, for example, P_{ad} is the *instantaneous difference* of the adiabatic vapour-space pressure from its equilibrium (time-averaged) value. In addition, all variables are assumed to oscillate with only *small fluctuations* around their time-averaged values.

2.2.2. Thermal domain – Linear Temperature Profile (LTP)

The thermal domain, which includes the complex time-varying two-phase heat transfer in heat exchangers, is the most critical part of the NIFTE, but it is also the least understood. In this domain, heat is converted into pressurisation and fluid flow, which acts as the driving process for the device. A number of *linear* models have been proposed for the two-phase heat transfer process that takes place between the heat exchangers and working fluid. One such model is the Linear Temperature Profile (LTP) model proposed originally in Refs. [3–5] without the inclusion of fluid inertia, and extended to include inertial effects by Markides and Smith [6] and Solanki et al. [7].

More recently, Solanki et al. [8] proposed two further models for the NIFTE, namely the Constant Temperature Difference (CTD) and Dynamic Heat Exchanger (DHX) models, by focussing specifically on two revised, but still linear, descriptions of the thermal domain. In a follow-up study [9] the same authors extended the linear LTP and DHX models to account for the exergetic losses that arise due to the irreversible fluctuating (zero-mean) heat transfer in the device, as reported in Ref. [5]. In the present study we use as our starting point the LTP model for the thermal domain with inertial effects included in the NIFTE fluid domain as presented in Refs. [6,7].

It is assumed in this model that the spatial temperature profile along the vertical walls of the heat exchangers $T_{hx}(z)$ is externally imposed as a boundary condition to the device and that it is static (or steady, i.e., it does not time-vary), as shown in Fig. 1b. It is also assumed that the convective heat transfer coefficient associated with phase change is considerably greater than that for the forced convection taking place away from an ‘active’ region near the vapour–liquid interface of the working fluid within which phase-change heat transfer occurs (see Fig. 2.14 on p. 67 in Ref. [5]). Denoting the instantaneous vapour–liquid interface level position

in the displacer cylinder by $y(t)$, the temperature on the heat exchanger wall that is experienced locally and instantaneously by the working fluid at the location of the active phase-change region is then $T_w(t) = T_{hx}(y(t))$. Under these conditions, the equation governing the exchange of heat between the working fluid and the heat exchangers is,

$$\dot{Q} = T_o \dot{S} = hA_s [T_w(t) - T_{ad}] \quad (4)$$

where \dot{Q} is the heat transferred per unit time and \dot{S} the associated rate of change of entropy, T_o is the equilibrium (time-averaged) temperature, h is the phase-change convective heat transfer coefficient (which is assumed to be constant), A_s is the surface area over which the heat transfer takes place, $T_w(t) = T_{hx}(y(t))$ is the heat exchanger wall temperature experienced by the working fluid at the position of the vapour–liquid interface $z = y(t)$, and T_{ad} is the temperature of the working fluid. It is further assumed that A_s is constant and equal to the multiple of the circumference of the heat exchanger blocks and the constant height of the active phase-change region, and that $T_w(y)$ is directly proportional to the vapour–liquid interface height in the displacer cylinder $y(t)$ [3–9].

Now, a connection is required between the thermal equation (Eq. (4)) and the fluid domain equations. This is done by ‘referring’ the thermal domain variables to the fluid domain: (i) the heat flow rate is converted to an equivalent volumetric flow-rate of vapour (due to phase change) via $\dot{S} = \rho_g s_{fg} U_{th}$, where ρ_g is the density of the vapour and s_{fg} is the specific entropy of vaporisation; and (ii) the temperatures are converted to pressures via $T_w = (dT/dP)_{sat} P_{th}$ and $T_{ad} = (dT/dP)_{sat} P_{ad}$, where $(dT/dP)_{sat}$ is the rate of change of working fluid temperature with pressure in the saturation region. Thus, and under the assumptions made above with respect to Eq. (4), this can then be re-written as,

$$U_{th} = \frac{P_{th} - P_{ad}}{R_{th}}; \quad R_{th} = \frac{\rho_g s_{fg} T_o}{hA_s (dT/dP)_{sat}} \quad (5)$$

where R_{th} is the thermal resistance between the working fluid and the walls of the heat exchangers. On applying electrical analogies between: (i) volumetric flow-rate (i.e., ‘referred’ entropy change

due to heat flow rate) and current; and (ii) pressure (i.e., 'referred' temperature) and voltage, the thermal equation governing heat exchange (Eq. (5)) becomes equivalent to Ohm's law, $I = \Delta E/R_{th}$.

This completes the modelling of the inertive LTP model for the NIFTE (NIFTE-LTP) and allows the circuit in Fig. 2a to be closed. Referring to Fig. 2a, which shows the LTP model employed in Refs. [6–8], and working in the Laplace domain, we can obtain two important functions:

$$U_{th} = \frac{P_{th}}{Z_{TOT}}; \quad Z_{TOT} \equiv R_{th} + [sC_{ad} + (Z_l + Z_{pfd})^{-1}]^{-1} \quad (6a)$$

$$P_d = G_{TF}P_{th}; \quad G_{TF} \equiv -(sC_d R_{th})^{-1} Z_{at} (Z_f + Z_d)^{-1} [1 + Z_{pfd}^{-1} (Z_{at} + Z_l)]^{-1} \quad (6b)$$

$$Z_{at}^{-1} = sC_{ad} + R_{th}^{-1}; \quad Z_{pfd}^{-1} = Z_p^{-1} + (Z_f + Z_d)^{-1}$$

Here, $Z_d = sL_d + 1/sC_d$ is the impedance of the displacer cylinder (representing flow inertia and hydrostatic pressure, respectively), $Z_f = R_f + sL_f$ is the impedance of the feedback connection (with the two terms representing flow drag and inertia, respectively), $Z_l = -R_l + sL_l$ is the impedance of the load (representing flow drag and inertia, respectively), and $Z_p = sL_p + 1/sC_p$ is the impedance of the power cylinder (representing flow inertia and hydrostatic pressure, respectively). These expressions contain the fluid domain electrical analogy parameters defined previously in (1)–(3). In addition, we have used the thermal resistance R_{th} , as defined in Eq. (5).

The first function (Eq. (6a)) is the total impedance Z_{TOT} that relates the referred 'thermal' pressure P_{th} (which is proportional to the temperature on the heat exchanger walls at the location of the active heat transfer region T_w) and the flow-rate as a result of the heat input (and hence, the mass input due to phase change) into the system U_{th} . The second function (Eq. (6b)) is the forward transfer function that relates the thermal pressure P_{th} to the hydrostatic pressure in the displacer cylinder $P_d = \rho g y$ (and hence, the liquid level height in the displacer cylinder y). Both expressions are obtained by combining the effects of the electrical components contained in the NIFTE-LTP circuit in Fig. 2a [6–8]. Once known, all necessary information about the system, such as efficiencies (defined in Section 2.5), etc., can be evaluated from these two functions.

In addition to the transfer function between P_{th} and P_d stated in Eq. (6b), there is an internal feedback loop in the NIFTE-LTP model that arises from the imposed temperature profile on the walls of the heat exchangers, specifically through a linear relationship ($T_w \propto y$) between the heat exchanger wall temperature at the location of the active heat transfer region $T_w(t) = T_{hx}(z)$ and the height of the vapour–liquid interface in the displacer cylinder $z = y(t)$ [3–9]. The constant of proportionality is equal to the temperature gradient along the heat exchanger walls ($c = dT_{hx}/dz$), which in turns scales with the ratio of the temperature difference between the heat exchangers to their respective vertical spatial separation. By extension, the internal feedback equation for the NIFTE-LTP

$$P_{th} = K_1 P_d \quad (7)$$

Eq. (7) linearly relates the thermal pressure P_{th} (i.e., the temperature of the heat exchanger walls at the active heat transfer region) to the hydrostatic pressure $P_d = \rho g y$ (i.e., liquid level height) in the displacer cylinder via the use of a constant of proportionality K_1 , also known as the 'feedback gain'.

At this point the set of equations that govern the operation of the NIFTE-LTP can be solved. Details of how this was done can be found in Section 2.3, and also in Refs. [6–9].

2.2.3. Thermal domain – Nonlinear Temperature Profile (NTP)

The NIFTE-NTP model introduces a nonlinearity in the two-phase heat transfer process between the heat exchanger and the working fluid. Specifically, based on the fact that the temperature on the heat exchanger walls T_{hx} cannot increase or decrease indefinitely with the vertical height in the heat exchanger blocks z (as allowed by the LTP model; see Fig. 1b), it assumes that T_{hx} (and consequently also, T_w) saturates when the liquid level in the displacer cylinder moves away from the equilibrium position (which lies halfway between the HHX and CHX), at some distance towards the ends of the heat exchangers. Fig. 1c shows a graphical representation of the specific NTP model used in this work for the vertical distribution profile of the heat exchanger wall temperature $T_{hx}(z) = \alpha \tanh(\beta z)$. As indicated, the (maximum) saturation amplitude in T_{hx} is denoted by α , while the slope at the origin is equal to $\alpha\beta$. Fig. 2b shows the electrical circuit representation of the NIFTE-NTP with the nonlinear heat exchanger temperature model. It can be seen that this is similar to the NIFTE-LTP (Fig. 2a), with the exception of the thermal domain on the left-hand side.

The thermodynamic state of this system can be specified by the minimum number of *independent* thermodynamic variables required to fully describe the system. The five thermodynamic variables that were chosen to describe the state of the circuit diagram in Fig. 2b are P_{ad} , P_d , P_p , U_f and U_p . These are the pressure in the vapour volume, the hydrostatic pressure in the displacer and pressure cylinders (due to the liquid heights), and the volumetric flow-rates in the feedback connection and pressure cylinder. A mathematical model of the circuit can be obtained in a similar way to the derivations relating to the linear equivalent in Section 2.2.2, by applying Kirchhoff's voltage and current laws to Fig. 2b [17]. Furthermore, here we non-dimensionalise the resulting set of ODEs, which yields the following set of five governing ODEs, one for each of the selected thermodynamic variables:

$$\frac{d\hat{P}_{ad}}{d\hat{t}} = \frac{\tau[K \tanh(\Lambda \hat{P}_d) - \hat{P}_{ad}]}{R_{th} C_{ad}} + \frac{\tau U_o (\hat{U}_f + \hat{U}_p)}{P_o C_{ad}} \quad (8a)$$

$$\frac{d\hat{P}_d}{d\hat{t}} = \frac{\tau U_o \hat{U}_f}{P_o C_d} \quad (8b)$$

$$\frac{d\hat{P}_p}{d\hat{t}} = \frac{\tau U_o \hat{U}_p}{P_o C_p} \quad (8c)$$

$$\frac{d\hat{U}_f}{d\hat{t}} = \frac{(\tau P_o / U_o) [L_l \hat{P}_p - L_p \hat{P}_{ad} - (L_p + L_l) \hat{P}_d] - \tau [L_l R_f + L_p (R_f + R_l)] \hat{U}_f - \tau L_p R_l \hat{U}_p}{L_l (L_d + L_f) + L_p (L_d + L_f + L_l)} \quad (8d)$$

$$\frac{d\hat{U}_p}{d\hat{t}} = \frac{(\tau P_o / U_o) [L_l \hat{P}_d - (L_d + L_f) \hat{P}_{ad} - (L_d + L_f + L_l) \hat{P}_p] + \tau [L_l R_f - (L_d + L_f) R_l] \hat{U}_f - \tau (L_d + L_f) R_l \hat{U}_p}{L_l (L_d + L_f) + L_p (L_d + L_f + L_l)} \quad (8e)$$

model as formulated in Fig. 2a (on the left-hand side of the circuit) in terms of pressures is,

The scaling parameters that were used to non-dimensionalise all thermodynamic variables (plus time) in these equations were chosen so as to allow the comparison of these variables with

physically relevant reference values. For instance, $P_o = 1.013$ bar was chosen as the scaling parameter for all pressure fluctuations, such that the pressure fluctuations in the system are referred to atmospheric pressure. The full set of scaling parameters and physical variables used can be found in Table 1, while Table 2 contains the relations used for the evaluation of the electrical parameters in Eqs. (8a)–(8e).

In addition, Table 3 summarises the nominal values (along with the corresponding investigated ranges used for the parametric study in Section 3.3) used for each electrical R , L and C parameter. The nominal values indicated in this table as “Set-I”

Table 1

Nominal values (in accordance with Markides and Smith [6] and Solanki et al. [7,8]) of the physical properties and variables that were employed in the present study, along with the scaling variables P_o, T_o, U_o and τ that were used in the non-dimensionalisation of the NIFTE-NTP system of ODEs (Eq. (8)), and the value of the nonlinear parameter A (normalised NTP parameter β). Also showing the corresponding investigated ranges (in accordance with Solanki et al. [7]) of the physical variables that were perturbed in the parametric study (Section 3.3).

| Variable | Nominal value | Investigated range | Units |
|----------------------------------|-----------------------|---|--------------------|
| A_d | 4.48×10^{-4} | 9.71×10^{-5} – 7.34×10^{-3} | m |
| A_f | 1.96×10^5 | 7.85×10^7 – 1.96×10^3 | m |
| A_l | 7.85×10^{-5} | 7.07×10^{-6} – 7.85×10^{-3} | m |
| A_p | 4.52×10^{-4} | 1.96×10^5 – 7.85×10^{-3} | m |
| A_s | 1.60×10^3 | 1.07×10^{-4} – 1.22×10^{-1} | m ² |
| d_f | 0.005 | 0.001–0.05 | m |
| d_l | 0.01 | 0.003–0.1 | m |
| g | 9.81 | – | m ² /s |
| h | 4.61×10^3 | 1.00×10^3 – 2.00×10^4 | W/m ² K |
| l_d | 0.26 | 0.2–2 | m |
| l_f | 0.15 | 0.05–0.5 | m |
| l_l | 1 | 0.01–30 | m |
| l_p | 0.55 | 0.2–2 | m |
| s_{fg} | 1.16×10^3 | – | J/kg K |
| $(\frac{dT}{dP})_{sat}$ | 28.9×10^{-5} | – | K/Pa |
| V_o | 1.94×10^{-4} | 2.37×10^{-5} – 2.25×10^{-2} | m ³ |
| γ | 1.09 | – | – |
| μ_l | 2.18×10^{-4} | – | kg/ms |
| μ_w | 1.00×10^{-3} | – | kg/ms |
| ρ_g | 2.98 | – | kg/m ³ |
| ρ_l | 621 | – | kg/m ³ |
| ρ_w | 998 | – | kg/m ³ |
| P_o | 1.013×10^5 | – | Pa |
| T_o | 309 | – | K |
| U_o | 8.00×10^4 | – | m ³ /s |
| τ | 5 | – | s |
| $A = \frac{\beta P_o}{\rho_l g}$ | 330 | – | – |

Table 2

Electrical analogy component definitions, in accordance with Markides and Smith [6] and Solanki et al. [7,8].

| Electrical element | Thermal-fluid effect | Component expression |
|---------------------|--|--|
| Resistance (R) | Feedback valve flow resistance (drag) | $R_f = 128\mu_l l_f / \pi d_f^4$ |
| | Load flow resistance (pressure/viscous drag) | $R_l = 128\mu_w l_l / \pi d_l^4$ |
| | Thermal resistance | $R_{th} = \rho_g s_{fg} T_o / h A_s (\frac{dT}{dP})_{sat}$ |
| Inductance (L) | Displacer cylinder inertia | $L_d = \rho_l l_d / A_d$ |
| | Feedback tube inertia | $L_f = \rho_l l_f / A_f$ |
| | Load inertia (fluid mass) | $L_l = \rho_w l_l / A_l$ |
| | Power cylinder inertia | $L_p = \rho_l l_p / A_p$ |
| Capacitance (C) | Vapour compressibility | $C_{ad} = V_o / \gamma P_o$ |
| | Displacer cylinder hydrostatic capacitance | $C_d = A_d / \rho_l g$ |
| | Power cylinder hydrostatic capacitance | $C_p = A_p / \rho_l g$ |

Table 3

Employed nominal values (“Set-I” in accordance with Markides and Smith [6] and Solanki et al. [7,8]; “Set-II” in accordance with Smith [3–5]) of the electrical components of the NIFTE-LTP and NIFTE-NTP models, and corresponding investigated ranges (in accordance with Solanki et al. [7]) used in the parametric study (Section 3.3). Based on the values of the physical properties and variables provided in Table 1 and the parameter definitions in Table 2.

| Electrical parameter | Nominal values | | Investigated range | Units |
|----------------------|-----------------------|-----------------------|--|-----------------------------------|
| | Set-I [6–8] | Set-II [3–5] | | |
| R_f | 2.13×10^6 | 2.17×10^7 | 7.10×10^1 – 4.44×10^9 | kg/m ⁴ s |
| R_l | 4.08×10^6 | 1.55×10^9 | 4.08×10^0 – 1.51×10^{10} | kg/m ⁴ s |
| R_{th} | 5.02×10^8 | 8.00×10^8 | 3.13×10^7 – 7.20×10^9 | kg/m ⁴ s |
| L_d | 1.80×10^5 | 1.58×10^{5a} | 8.50×10^3 – 7.01×10^6 | kg/m ⁴ |
| L_f | 4.74×10^6 | 4.74×10^{6a} | 1.57×10^4 – 3.95×10^8 | kg/m ⁴ |
| L_l | 1.27×10^7 | 1.51×10^{7a} | 1.27×10^3 – 4.24×10^9 | kg/m ⁴ |
| L_p | 3.77×10^5 | 3.77×10^{5a} | 7.90×10^3 – 3.16×10^7 | kg/m ⁴ |
| C_{ad} | 1.76×10^9 | 3.70×10^{-9} | 9.84×10^{11} – 1.40×10^7 | m ⁴ s ² /kg |
| C_d | 7.35×10^8 | 2.15×10^{7b} | 1.44×10^{-8} – 1.20×10^6 | m ⁴ s ² /kg |
| C_p | 7.43×10^{-8} | 7.38×10^{-8} | 3.22×10^{-9} – 1.29×10^6 | m ⁴ s ² /kg |

^a No inductance (i.e., inertia) parameter values are provided in Refs. [3–5]. The inductance values used in the present study were calculated from the definitions in Table 2, and the description of the experiments on the NIFTE prototype in Refs. [3–5].

^b A value for the nominal hydrostatic capacitance in the displacer cylinder C_d was not stated in Refs. [3–5], other than to state that this parameter should be within the range from 7.59×10^{-8} to 2.15×10^{-7} m⁴ s²/kg. The value of C_d used in the present study was chosen for consistency with our definition of C_p .

parameters are calculated based on the values of the physical properties and variables in Table 1. The values of the physical variables stated in Table 1, and hence also the Set-I nominal parameters stated in Table 3, correspond to the configuration of a working prototype of the NIFTE as presented in Refs. [6–8], while the investigated ranges give the values of the parameters when they are perturbed within a reasonable range from the NIFTE prototype, again consistent with the efforts in Refs. [6,7]. In particular, the Set-I nominal load corresponds to a delivery pipe 1 m long and with a diameter of 0.01 m that would in practice be connecting a supply tank of water to the destination tank. The Set-II nominal parameters, which are also contained in Table 3, are only used for the model validation effort presented in Section 3.2.

At this stage the set of five ODEs (Eqs. (8a)–(8e)) that govern the operation of the NIFTE can be solved for the five thermodynamic variables, given values for the parameters K and A in Eq. (8a). Details of how this was done are included in Section 2.4. Based on the results, it is then possible to investigate the performance of the NIFTE-NTP model as a function of K and A . The dimensionless parameter K is the ‘nonlinear gain’ and is defined with respect to the other known parameters through,

$$K = \frac{\alpha}{P_o (\frac{dT}{dP})_{sat}} = \frac{\alpha}{T_o (\frac{dT}{dP})_{sat}}; \alpha = \frac{\Delta T_{hx}}{2} \tag{9}$$

Recall, from Fig. 1c, that α is the maximum (saturation) temperature amplitude on the heat exchanger walls. In addition, $(dT/dP)_{sat}$ is the change of dimensionless temperature per unit of dimensionless pressure in the two-phase saturation region, and T_o is the temperature of the working fluid at equilibrium (time-mean) conditions. The expression in Eq. (9) indicates that the nonlinear gain K is proportional to α , and thus, it implies that K is proportional to the maximum available fluctuation in (or, amplitude of) the working fluid temperature in contact with the heat exchangers, which in turn scales with the temperature difference between the two heat exchangers.

Likewise, the dimensionless parameter A in Eq. (8a) is a function of parameter β that in turn depends on the slope at the origin in the plot of T_{hx} against z (see Fig. 1c), and can be expressed as,

$$\mathcal{A} = \frac{\beta P_o}{\rho_i g} \quad (10)$$

The chosen value of β ($\approx 20 \text{ m}^{-1}$) that was employed throughout this study can be found in Appendix A. This value of β corresponds from Eq. (10) to a value for $\mathcal{A} = 330$ (as stated in Table 1).

2.3. NIFTE-LTP model solution

The stability of a linear system can be investigated by studying its closed loop transfer function (CLTF) [18]. The performance of the system is then evaluated at marginal stability conditions [6–9]. The marginal stability condition of the NIFTE-LTP model involves the solution of the system of equations that relate P_{th} and P_d (i.e., Eqs. (6) and (7)) such that the output is purely oscillatory with a constant amplitude. The CLTF $C(s)$ corresponding to the NIFTE-LTP model in Fig. 2a is given by,

$$C(s) = \frac{G_{TF}(s)}{1 - K_1 G_{TF}(s)} \quad (11)$$

where $G_{TF}(s)$ is the forward transfer function relating the input pressure P_{th} to the output pressure P_d defined in Eq. (6b), and K_1 is the feedback gain that relates P_d back to P_{th} (Eq. (7)).

The stability of the NIFTE-LTP model at a given value of feedback gain K_1 is found by observing the (complex) poles of the CLTF of this system, that is, the (complex) solutions of the polynomial equation in s that results from setting the denominator of $C(s)$ to zero. The poles $s_i = \sigma_i \pm i\omega_i$ are either purely real ($\omega_i = 0$) or appear in complex conjugate pairs. Each purely real pole (or, system eigenvalue) represents a growing or decaying exponential, while each complex eigenvalue pole (or, eigenvalue) pair represents a single-frequency periodic oscillation (i.e., pure sinusoid with frequency ω_i) whose amplitude can either grow ($\sigma_i > 0$) or decay ($\sigma_i < 0$) exponentially, in the time response of the system. As in any linear system with multiple eigenvalues, the overall system response of the NIFTE-LTP model is a linear superposition of the responses represented by each eigenvalue. The response obtained in this way is the same as that obtained by solving directly (without the use of electrical analogies leading to circuit diagrams) the linear ODEs that model the system.

The solution of the NIFTE-LTP model results in a total of five eigenvalues, including two complex conjugate eigenvalue pairs and one real eigenvalue. Marginal stability occurs when one complex eigenvalue pair lies on the imaginary axis and all other eigenvalues have negative real parts. In these conditions all stable (decaying) responses of the eigenvalues with negative real parts die away and the long-term behaviour of the system becomes dominated by the marginal eigenvalue pair whose associated response is oscillatory with a constant amplitude. The primary performance indicators, such as the engine's oscillation frequency and associated exergetic efficiency, are then evaluated at marginal stability, as is the value of the feedback gain K_1 and associated temperature gradient dT_w/dy in the HHX and CHX that ensures that the marginal stability condition is met.

In previous studies it was found that liquid flow inertia is important to leading order in the modelling of the NIFTE [7] and that the operation of the engine is sensitive to certain parameters, such as the resistance (representing the flow drag) in the feedback connection and the capacitance (representing the cross-sectional area) in the power cylinder [8]. In fact, a systematic sensitivity analysis in Ref. [6] identified the feedback connection, the power cylinder, the adiabatic volume and the thermal resistance in the heat exchangers as the components that need the most attention in order to optimise the operation of the NIFTE in terms of efficiency [6]. The findings of the linear NIFTE model studies form an important basis for comparison with the present effort.

2.4. NIFTE-NTP model solution

All of the NIFTE-LTP equations are linear and, as such, the resulting system can only exhibit one of three behaviours, depending on the value of the feedback gain K_1 : asymptotic stability, instability and marginal stability. At low values of K_1 the system is asymptotically stable and the amplitude of the corresponding solution (or, output) decreases exponentially, even if this exponential decay is oscillatory. Increasing the value of K_1 leads to a critical threshold value at which the system becomes marginally stable and *non-robust* oscillations can be observed. By *non-robust*, we mean that, at this condition, any slight disturbance or infinitesimally small change in K_1 will cause the system to either become stable or unstable. For values of K_1 above this threshold limit the system is unstable and the amplitude of the corresponding solution grows exponentially. From experimental observations it was confirmed that the NIFTE prototype undergoes robust sustained oscillations, even when the gain is increased further [3–5]. This is known as limit cycle behaviour and can only be explained by taking into account explicitly the nonlinear nature of the device. This is the main aim of the present effort.

2.4.1. Critical gain and Hopf bifurcation point: numerical bifurcation analysis

We return to Eqs. (8) to (10), which describe fully the nonlinear NIFTE-NTP model. When the value of the nonlinear gain K in Eq. (8a) (which scales with the temperature difference between the heat exchangers as discussed below Eq. (9)) is small, the system reaches an equilibrium that can be shown to be *locally asymptotically stable*, since the values of the real parts of all five eigenvalues are negative. As K increases beyond a critical value K^* (which corresponds to the critical parameter value at which a Hopf bifurcation⁴ occurs, see next section), a pair of complex conjugate eigenvalues cross the imaginary axis with non-zero speed and, as a consequence, the system becomes locally unstable. Performing a numerical bifurcation analysis and numerical time simulations (see Section 3.1), the solution can be shown to converge to an emergent (locally) attractive limit cycle [19].

MatCont, a numerical continuation toolbox for bifurcation analysis in MATLAB, was used to calculate the critical value K^* of the nonlinear gain K at the Hopf bifurcation point where limit cycle behaviour is achieved with the minimum gain, and hence also, the minimum temperature difference between the two heat exchangers. In addition, the behaviour of the system was investigated for values of K 'slightly' greater than the critical bifurcation value K^* . The frequency of oscillation of the system and its exergetic efficiency were also evaluated for values of $K = K^*$ and 'slightly' above.

Numerical continuation algorithms such as MatCont are based on the following working principle: given a first-order, but nonlinear dynamical system $\dot{x} = f(x, \theta)$, where $f(\cdot, \cdot) : \mathbb{R}^n \times \mathbb{R}^p \rightarrow \mathbb{R}^n$ is a continuous function of both x and θ , and given initial parameter values θ_0 and an associated equilibrium point x_0 that is the solution of the equation $f(x_0, \theta_0) = 0$, MatCont calculates the evolution of the equilibrium values as the value of the bifurcation parameter is modified by small increments [20]. This is known as an equilibrium continuation process. In performing the numerical continuation MatCont employs standard ODE solvers in MATLAB, which use variable sampling step sizes for the numerical integration to obtain the best error/speed of convergence compromise.

The values of the electrical parameters presented in Table 3, to-

⁴ At the Hopf bifurcation point (e.g., Fig. 3a) the real part of a pair of complex conjugate eigenvalues is zero, and the angular frequency of oscillation ω of the solution at the Hopf bifurcation point is given by the imaginary part of the pair of purely imaginary eigenvalues, i.e., $\omega = \Im(\lambda_1) = -\Im(\lambda_2)$; where $\lambda_1 = i\omega$, $\lambda_2 = -i\omega$.

gether with equilibrium values for all five independent thermodynamic variables (P_{ad} , P_d , P_p , U_f and U_p) set to zero and the nonlinear parameter λ (see Eq. (10)) set to 330, were used to initialise the equilibrium continuation process in MatCont. With these initial values, the numerical continuation method reveals the existence of a Hopf bifurcation point and the subsequent emergence of an asymptotically stable limit cycle for values of $K > K^*$. The expression for the critical K^* in terms of other known physical parameters is,

$$K^* = \frac{\alpha^*}{P_o(d\bar{T}/dP)_{sat}} = \frac{\alpha^*}{T_o(d\bar{T}/d\bar{P})_{sat}}, \quad (12)$$

where α^* is the critical saturation amplitude on the heat exchanger walls at the Hopf bifurcation point. The value of K^* associated with the Set-I nominal parameter values (see Tables 3 and 4) is 0.098 and this corresponds to a temperature difference of about 5.7 K between the two heat exchangers.

2.4.2. System time-response: solution of ODEs via numerical integration

The numerical integration of the NIFTE-NTP model described by the nonlinear ODEs in Eq. (8) was performed using the variable step size Runge–Kutta numerical solver ode45 available by default in MATLAB. The ode45 solver is based on an explicit Runge–Kutta (4,5) formula, also known as the Dormand–Prince pair [21]. It is a one-step solver, that is, in computing the value of the thermodynamic state variable x_i at time-step n , $x_i(t_n)$, it requires only the solution of the independent thermodynamic state variables at the immediately preceding time instant, $\underline{x}(t_{n-1})$. Having solved the NIFTE-NTP system of ODEs and recovered the dynamic response of the NTP model, a single oscillation cycle is extracted and from it a number of key metrics characterising their numerical solutions are evaluated, namely the oscillation frequency and the exergetic efficiency.

2.5. Exergetic efficiency evaluation

Thermal efficiency is a primary measure of the thermodynamic performance of heat engines. It is a strong function of the temperature at which heat is available to the heat engine. An improved performance indicator involves a comparison of the thermal efficiency of a heat engine with the efficiency of an equivalent Carnot engine operating between the same hot source and cold sink temperatures. This quantity is known as the exergetic efficiency and it is defined as the ratio of the thermal efficiency of the heat engine to that of the equivalent Carnot cycle [1,22]. Unlike the thermal efficiency, the exergetic efficiency of heat engines operating across different temperature differences can be compared meaningfully. Given that the heat source for the NIFTE is low-grade heat (heat available at low temperature, and also typically, at little cost), the Carnot efficiency will be inherently low. The exergetic efficiency is used herein as the preferred performance indicator.

Two exergetic efficiencies can be defined for the NIFTE: the device exergetic efficiency, and the system exergetic efficiency [6]. The exergetic efficiency of the device is the work done in the load (in the form of liquid pumping) relative to the exergy input into the system, which is a measure of the total work potential of the cycle undergone by the NIFTE. On the other hand, the exergetic efficiency of the system is the work done in the load and dissipated parasitically in the engine's feedback tube (#6 in Fig. 1a) relative to the exergy input into the system. Mathematically, the two exergetic efficiencies are defined as:

$$\eta_{ex,dev} = \frac{\overline{P_l(t)U_l(t)}}{\overline{P_{th}(t)U_{th}(t)}} = \frac{\oint P_l dV_l}{\oint P_{th} dV_{th}} \quad (13a)$$

$$\eta_{ex,sys} = \frac{\overline{P_l(t)U_l(t)} + \overline{P_f(t)U_f(t)}}{\overline{P_{th}(t)U_{th}(t)}} = \frac{\oint P_l dV_l + \oint P_f dV_f}{\oint P_{th} dV_{th}} \quad (13b)$$

where P_f , P_l and P_{th} are the feedback, load and input thermal pressures respectively, while V_f , V_l and V_{th} are the volume of the working fluid in the feedback tube, the volume in the load, and the volume associated with phase change. Recall that U_f , U_l and U_{th} are the volumetric flow-rate through the feedback tube, the volumetric flow-rate of the load, and the volumetric flow-rate due to phase change.

The device exergetic efficiency $\eta_{ex,dev}$ is the time-averaged power dissipated at the load relative to the total time-averaged power into the electrical circuit, according to Eq. (13a). This can be found by integrating $P_l dV_l$ and $P_{th} dV_{th}$ numerically over one engine cycle period. A similar procedure is followed to obtain the system exergetic efficiency $\eta_{ex,sys}$, i.e., by integrating numerically $P_l dV_l$, $P_f dV_f$ and $P_{th} dV_{th}$ over one engine cycle period and using Eq. (13b).

3. Results and discussion

3.1. Operation with nominal parameters

The LTP and NTP models were presented in Sections 2.2.2 and 2.2.3, respectively. This section focuses on the operation of the NTP model when using the nominal values of the electrical R , L and C parameters. When referring to nominal values throughout this section, unless otherwise stated, we refer specifically to those values identified as “Set-I” in Table 3, in accordance with Markides and Smith [6] and Solanki et al. [7,8]. As mentioned earlier, the Set-I nominal values are based on a physical manifestation of the NIFTE represented by values of the physical variables in a working prototype of the NIFTE described in Refs. [6–8] and summarised in Table 1.

3.1.1. Bifurcation analysis through numerical continuation

The bifurcation diagram for the NIFTE operating with all parameters at their nominal values is shown in Fig. 3a. A bifurcation diagram is a plot that shows the qualitative change in the equilibrium of a dynamical system when the value of a control parameter (also known as a bifurcation parameter) is varied [19]. For the NIFTE, it is a plot of a thermodynamic variable (here the displacer pressure P_d)

Table 4

Validation of NIFTE-NTP model with parameters set to the nominal value sets contained in Table 3 (“Set-I” in accordance with Markides and Smith [6] and Solanki et al. [7,8]; “Set-II” in accordance with Smith [3–5]) and with the NTP parameter $\lambda = 330$.

| Model prediction | Oscillation frequency, f_o (Hz) | Exergetic efficiency | | Marginal/critical gain | |
|------------------|-----------------------------------|--|--|-----------------------------------|----------------------|
| | | Device efficiency, $\eta_{ex,dev}$ (%) | System efficiency, $\eta_{ex,sys}$ (%) | $\frac{dT_{hx}}{d\lambda}$ (K/cm) | ΔT_{hx} (K) |
| NTP/Set-I | 0.36 | 0.95 | 3.9 | 0.57 | 5.7 |
| NTP/Set-II | 0.098 | 12.4 | 12.5 | 13.7 | 137 |
| LTP/Set-I | 0.36 | 0.95 | 3.9 | 0.57 | 0.2–4.5 ^a |
| LTP/Set-II | 0.098 | 12.4 | 12.5 | 13.6 | 4.8–107 ^a |

^a The minimum value is based on the gap between the two heat exchanger blocks of 3–4 mm [5]. The maximum value is based on the same gap between the two heat exchanger blocks, plus a half-height of the heat exchanger blocks of 75 mm (90 mm for the HHX and 60 mm for the CHX) [5].

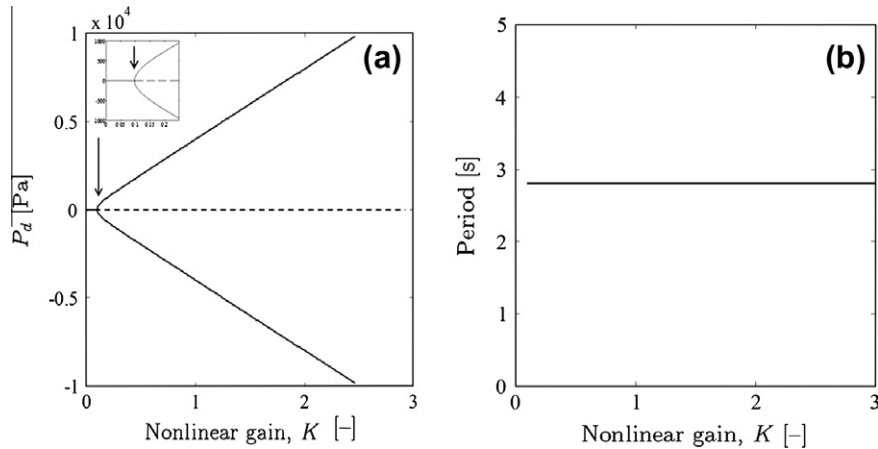


Fig. 3. (a) Bifurcation diagram for the nominal NIFTE. It gives the qualitative asymptotic behaviour of the system when a control parameter (the nonlinear K gain in this case) is varied. The arrow is pointing to the Hopf bifurcation point which occurs at the critical value of the nonlinear gain, $K^* = 0.098$. To the left of the arrow is a continuous horizontal line (seen more clearly in the inset) that represents the position of the locally stable equilibrium point. Beyond the critical value K^* , the equilibrium point becomes locally unstable and the continuous horizontal line bifurcates to give the maximum and minimum amplitude of the limit cycle (as seen through the state variable P_d). The dashed horizontal line represents the position of the locally unstable equilibrium that exists for values of K larger than K^* . (b) Period of oscillation for the Set-1 nominal NIFTE against nonlinear gain K .

against the nonlinear gain K and it shows how the stable equilibrium of the NIFTE becomes locally unstable when a critical value K^* of the nonlinear gain K is reached. The equilibrium point is stable for values of the gain K lower than $K^* = 0.098$, but becomes locally unstable at values of K larger than K^* . In other words, and referring specifically to Fig. 3a, for $K < K^*$ the NIFTE is at a stable equilibrium and does not operate (i.e., it does not oscillate). On the other hand, for $K > K^*$ the NIFTE undergoes limit cycle oscillations with an amplitude that increases monotonically as K increases.

As we have shown numerically using MatCont, for values of K larger than K^* , the nonlinear system exhibits asymptotically stable limit cycle oscillations around the locally unstable equilibrium point. In energetic terms, the critical bifurcation value K^* corresponds to the *minimum* temperature difference between the hot and cold heat exchangers required to achieve sustained limit cycle oscillations. Therefore, as stated in Section 2.4.1 and Table 4, the value of K^* corresponds here to a minimum temperature difference of $\Delta T_{hx} = 5.7$ K between the two heat exchangers for operation, from Eq. (9). The amplitude of the oscillations grows as the gain K is increased. This occurs physically in the actual NIFTE pumping

device by increasing the temperature difference between the heat exchangers ΔT_{hx} .

3.1.2. Amplitude and frequency of oscillation

The amplitude and frequency of oscillation are two important properties that define an oscillating system. Fig. 3b shows the relationship between the period of oscillations and the nonlinear gain K . Interestingly, it can be seen that for a given model configuration (that is, for a given set of electrical parameters R , L and C), the period and therefore the frequency of oscillation f_o are independent of the temperature difference between the heat exchangers ΔT_{hx} .

The effect of the temperature difference between the heat exchangers ΔT_{hx} on the oscillation amplitudes of the five selected thermodynamic pressure and flow-rate variables is shown in Fig. 4. It was found, from Fig. 3a, that when K is increased beyond the critical value K^* , the amplitude of oscillation increases parabolically as the temperature difference increases in the immediate vicinity of the bifurcation point. This is a standard observation for a Hopf bifurcation point. However, further away from the bifurcation point, Fig. 4 shows that the amplitudes of oscillation vary linearly with the nonlinear gain K (i.e., the temperature difference

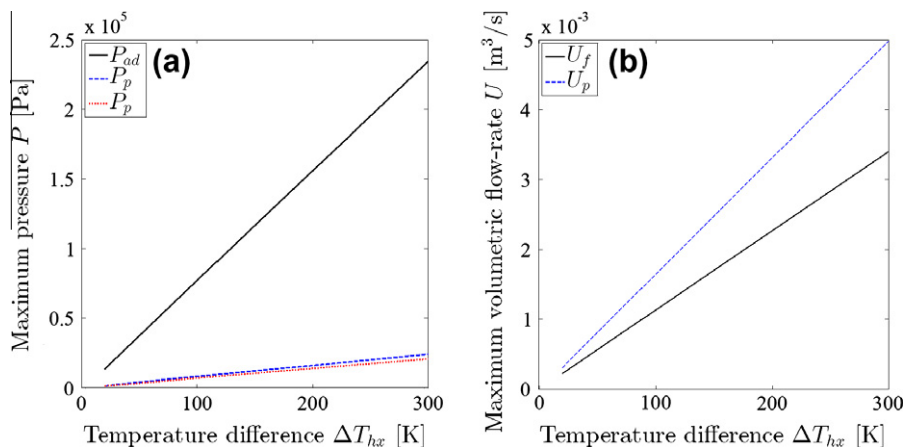


Fig. 4. Maximum amplitude of: (a) the pressure oscillations, and (b) the flow-rate oscillations in various components against the temperature difference between the heat exchangers ΔT_{hx} .

between the HHX and CHX). This linearity is a particular non-trivial characteristic of the NIFTE-NTP model.

Hence, two important conclusions can be drawn at this point:

1. The amplitudes and frequency of the oscillations of the thermodynamic properties and heat and fluid flow (pumping) variables can be controlled/adjusted independently of each other, and specifically;
2. The amplitudes grow *linearly* with K (i.e., the heat exchanger temperature difference) whereas the frequency is independent of K , but is a function of other device parameters.

This has the following very powerful consequences in terms of design:

1. The fluctuating amplitudes of the properties/variables can be scaled in proportion to the temperature difference that is established in the heat exchangers, and;
2. Once these have been set, the frequency of oscillation can be adjusted by choosing the right set of physical (materials, construction) parameters for the NIFTE pump.

3.1.3. Dynamic system response time-simulation

The NIFTE was reported in Ref. [5] as operating across a temperature difference between its heat exchangers of approximately 80 K. In order to examine the dynamic behaviour of the system at this condition, a value of $K = 1.37$, which corresponds to a temperature difference of 80 K, was used to run time simulations for

the NIFTE-NTP model. The results of this simulation are shown in Fig. 5.

In Fig. 5a it can be seen that the pressures in the displacer cylinder P_d and power cylinder P_p are sinusoidal, whereas the pressure in the adiabatic region P_{ad} exhibits a ‘beating’ phenomenon. This is the first instance of a model of the NIFTE pump that has been capable of predicting this type of behaviour, which is fundamentally different from what is observable in the response of the linear models where all the thermodynamic variables vary sinusoidally with time. The beating phenomenon has been observed experimentally in the same conditions (see Fig. 4.6 on p. 138 in Ref. [5]).

The temporal evolutions of the volumetric flow-rates in the feedback tube U_f , the load U_l and the power cylinder U_p , are shown in Fig. 5b. Only the volumetric flow-rate of the working fluid through the feedback tube U_f is a pure sinusoid. This is expected as the volumetric flow-rate through the feedback tube is equal to the flow-rate in the displacer cylinder (see Fig. 2b). Since the pressure in the displacer cylinder P_d is a sinusoid (Fig. 5a), the flow-rate in the displacer cylinder and therefore the feedback tube U_f must also be sinusoids. The flow-rate into the load U_l is the most important flow-rate variable to the user, as it determines the pumping capability of the NIFTE. Again, this exhibits a ‘beating’ phenomenon, which is a type of behaviour that is not predicted by any of the linear models. As a final comment it is pointed out, as demonstrated by Fig. 5c and also by the thermodynamic cycle diagrams in Fig. 7, that beating is not always observed by the NIFTE-NTP. In fact, Set-II nominal values do not give rise to such behaviour, though clearly the oscillations are still not sinusoidal as would be predicted by the linear models.

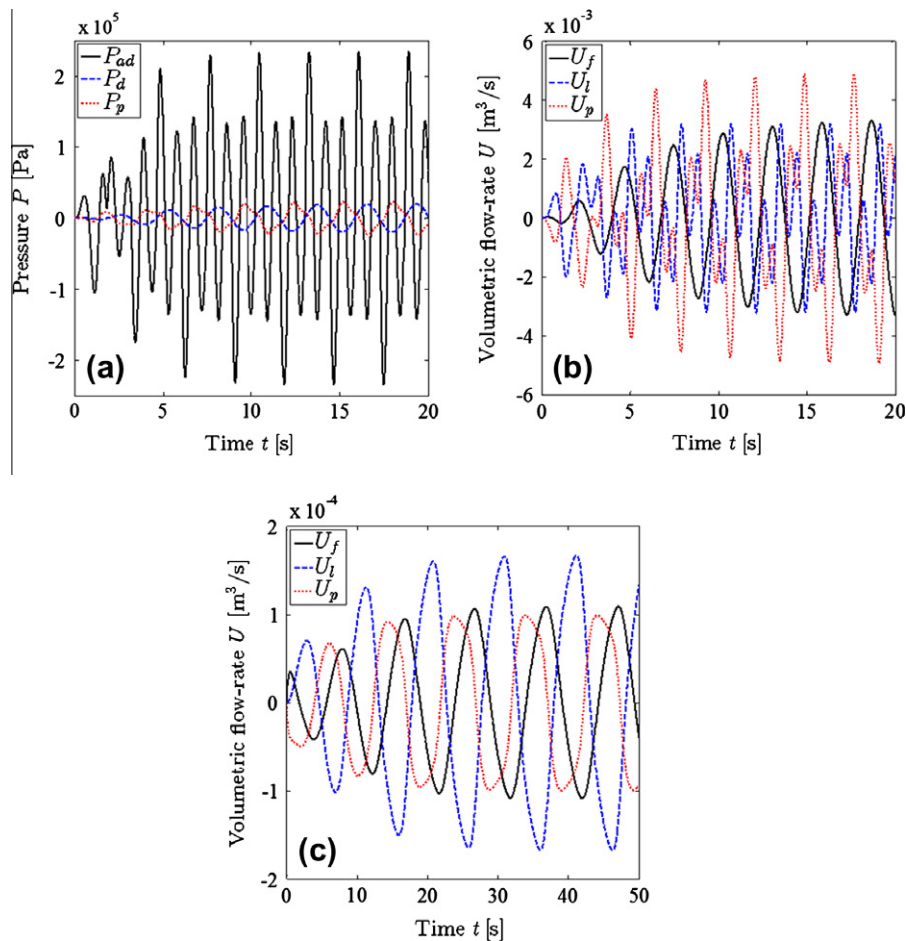


Fig. 5. (a) Pressures and (b) volumetric flow-rates against time, in various components. Both for Set-I nominal parameters. (c) Repeat of (b), but for Set-II nominal parameters.

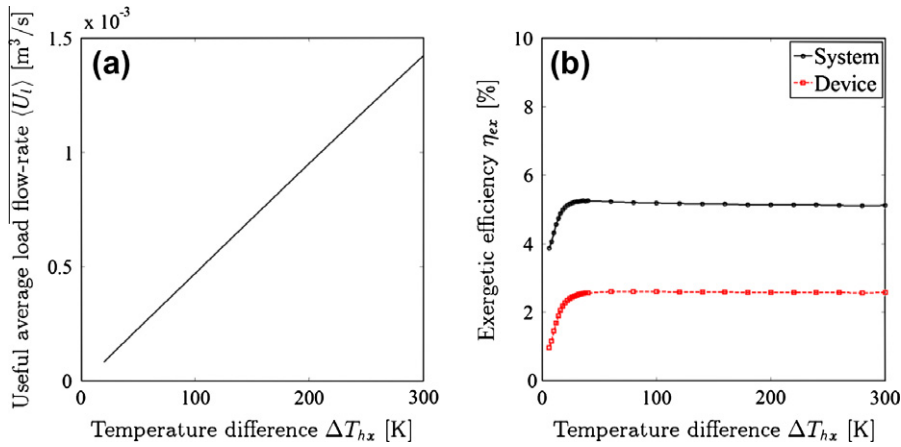


Fig. 6. (a) Useful average volumetric flow-rate $\langle U_l \rangle$, and (b) exergetic efficiency measures η_{ex} against the temperature difference between the heat exchangers ΔT_{hx} .

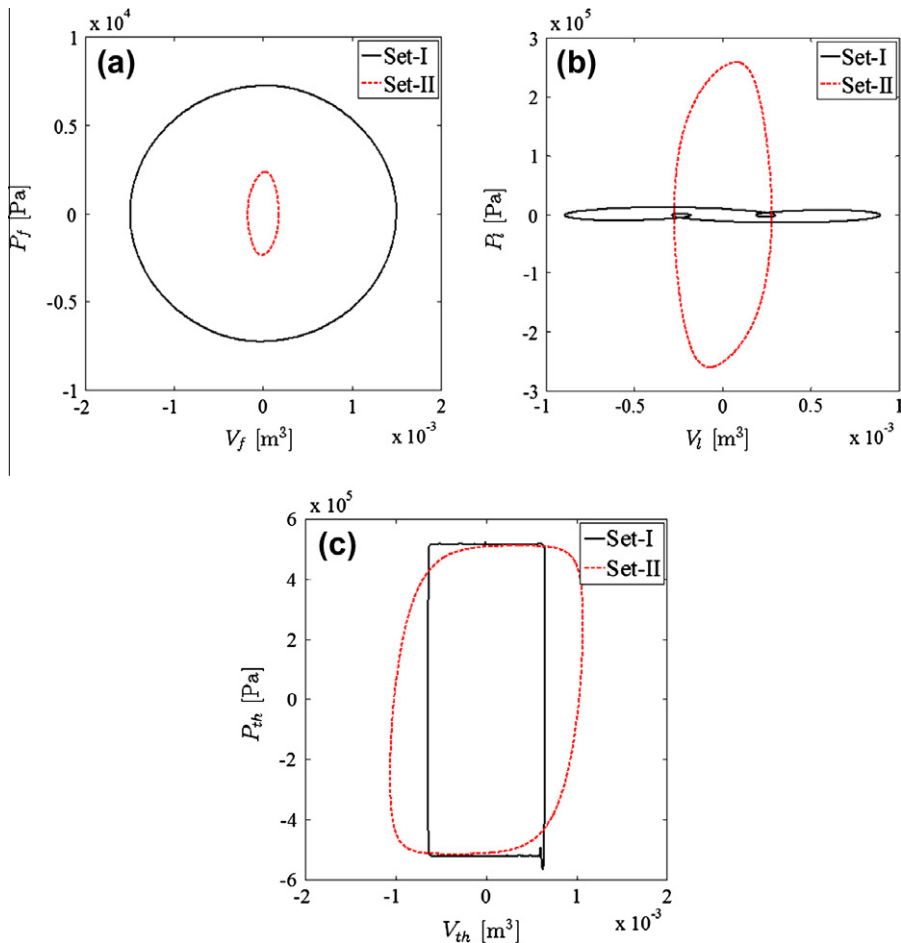


Fig. 7. (a) Feedback pressure P_f vs. volume of working fluid V_f for one period of oscillation. (b) Load pressure P_l vs. volume into the load V_l . (c) Input thermal pressure P_{th} vs. volume generated as a result of evaporation V_{th} . Showing results for both sets of nominal parameter values (from Table 3).

3.1.4. Useful flow-rate and exergetic efficiency

It was mentioned above that the average volumetric flow-rate of the liquid being pumped is a quantity that is of prime importance to the designer and user of the NIFTE device. The useful time-average volumetric flow-rate is the total volume of liquid pumped from the pump into the load during the half-cycle when liquid is displaced out of the device over the complete cycle period. The effect of the temperature difference between the heat exchangers on the useful average volumetric flow-rate is shown

in Fig. 6a, where it is evident that the useful average volumetric flow-rate through the load is directly proportional to the HHX-CHX temperature difference. Clearly, there is an incentive to use as high a temperature difference as possible across the NIFTE, though this will be limited by the external heat source and heat sink temperatures with which the NIFTE will interface thermally.

Based on our proposed nonlinear model, Eqs. (13a) and (13b) were used to evaluate the system and device exergetic efficiencies of the NIFTE for the nominal pump configuration at varying

nonlinear gains and hence HHX-CHX temperature differences. The results are shown in Fig. 6b and were obtained by evaluating the areas enclosed inside the Lissajous plots in Fig. 7a–c. In particular, the integrals of these three plots are equal to: the work dissipated parasitically in the feedback tube; the useful work done in the load; and the total exergy input (work potential) to the system, respectively, over a complete cycle of oscillation [6,22]. The exergetic system and device efficiencies $\eta_{ex,sys}$ and $\eta_{ex,dev}$ were evaluated using the appropriate quantities according to Eqs. (13a) and (13b). For instance, the system exergetic efficiency $\eta_{ex,sys}$ is the ratio of the work done in the load to the work input into the NIFTE.

The effect of the HHX-CHX temperature difference ΔT_{hx} on both exergetic efficiencies is shown in Fig. 6b. This plot indicates that the device $\eta_{ex,dev}$ and system $\eta_{ex,sys}$ exergetic efficiencies are fairly constant with an increasing ΔT_{hx} over the temperature range from 30 K and higher, which reflects temperatures of low- to medium-grade heat sources up to ~ 300 °C. However, at temperature differences lower than 30 K, and down to the critical (minimum) ΔT_{hx} of ~ 6 K, both efficiencies drop quickly and approach their nominal values, which are 0.95% and 3.9% for the device and system exergetic efficiency, respectively (see Set-I results in Table 4). It can be deduced from Fig. 6b that neither of the two exergetic efficiencies are a strong function of the temperature difference across the device for heat source temperatures at and greater than 40–50 K or so, unlike the average volumetric flow-rate which shows a significant improvement with increasing ΔT_{hx} . This can be explained by considering that at larger temperature differences both the total exergy (work) input as well as the work done in the load increase, while their ratio remains approximately the same. On the other hand, for very low temperature heat sources, which are near the critical ΔT_{hx} , the efficiency will show a rapid improvement initially, before levelling off due to the effect of the saturation in the nonlinearity.

3.2. Model validation

Before proceeding to the parametric investigation based on the nonlinear NIFTE-NTP model that immediately follows the current section (in Section 3.3), it is important to compare quantitatively the results from this revised model with: (i) results relating to nominal NIFTE configurations for the limiting case of near-critical gain, when we expect the results to tend towards the predictions of the linear NIFTE-LTP model in marginally stable conditions (Section 3.2.1); (ii) both NIFTE-LTP model predictions and experimental data that have been made available from earlier studies [3–5] for the variations of key performance indicators (specifically the oscillation frequencies f_o and engine efficiencies η_{ex}) when important device parameters (specifically the feedback and load resistances R_f and R_l) are perturbed from their nominal values (Section 3.2.2); and (iii) experimental data on the amplitudes and relative phases of key thermodynamic properties and the measured thermodynamic cycles (specifically P – V diagrams) from the same experimental studies (Section 3.2.3).

3.2.1. Comparisons with the nominal NIFTE-LTP

Firstly, the predictions from the NIFTE-NTP model with the nonlinear bifurcation parameter K set to a value ‘slightly’ greater than its critical value K^* are compared to the corresponding predictions generated by the NIFTE-LTP for a nominal configuration. Two sets of nominal R , L and C parameter values are employed here, both of which are stated in Table 3. Set-I nominal values correspond to the configuration of a working prototype of the NIFTE as suggested in Refs. [6–8], while Set-II nominal values are taken directly from Ref. [5], which reported on the construction and testing of the NIFTE prototype pump, and where an early effort was made to evaluate these parameters experimentally.

The outcome of our nominal system comparison is summarised in Table 4. Note that, in this table the values of the HHX-CHX temperature differences ΔT_{hx} in the LTP column are approximate estimates, based on the marginal stability gain (i.e. heat exchanger temperature gradient dT_{hx}/dz) and an indicative length between the two heat exchangers. The minimum length is taken as the physical gap between the two heat exchanger blocks, reported as being 3–4 mm in Ref. [5]. The maximum length is taken as 75 mm (plus the gap), which is the half-height of the combined HHX and CHX blocks that were 90 mm and 60 mm long, respectively. The agreement between the two models with regards to the oscillation frequency, the two exergetic efficiencies, and the ‘near-critical’/marginal (minimum) gain required for oscillation is excellent, as would be expected at low nonlinear gains, reflecting a correct implementation of the NIFTE-NTP model. Interestingly the two measures of efficiency, namely the device $\eta_{ex,dev}$ and system $\eta_{ex,sys}$ exergetic efficiency, are different for the Set-I nominal system, but similar for the Set-II system. In addition, the Set-II system shows considerably higher efficiencies. The most significant difference between the two sets of nominal values is the three orders of magnitude change in R_l . On this evidence it can be suggested that most of the exergy in the Set-II system is dissipated in the load, which would also explain the significantly lower frequencies of operation f_o . In a practical setting both of these performance indicators would be important in determining the eventual flow-rate capability of the NIFTE.

3.2.2. Variations of performance indicators

Having investigated the LTP and NTP two nominal configurations of the NIFTE in the previous section, Fig. 8a–c shows results from the linear and nonlinear models, in both cases compared to experimental data points taken from Ref. [5] (in particular Figs. 4.15–4.21 on p. 151–160). In these plots one can examine the variations of the oscillation frequency f_o and engine exergetic efficiency η_{ex} when the feedback and load resistances R_f and R_l are perturbed from their Set-II nominal values, with $K = 3.41$ ($\Delta T_{hx} = 200$ K) and $\mathcal{A} = 330$. Recall, from Table 4, that the critical value of the bifurcation parameter was $K^* = 2.34$ ($\Delta T_{hx} = 137$ K).

It can be seen in Fig. 8a–c that the trends for the investigated quantities are captured, and that the reported magnitudes of the performance indicators are reasonable considering the uncertainty in the evaluation of the electrical parameters and the experimental errors associated with the data points (these are estimated as being of the order of $\pm 20\%$, being dominated by the error in the volumetric displacement measurement⁵). Also shown are two additional trend lines for higher R_{th} , which demonstrate an improved prediction of the frequency f_o and device efficiency $\eta_{ex,dev}$. This suggests that, either this parameter has been significantly under-predicted, or one or more exergy loss mechanisms are absent from the description of the engine. Nevertheless, the overall agreement with the experimental data is sufficient to allow predictions with some confidence, without the necessity to include additional complexity into the current model.

3.2.3. Thermodynamic properties and cycles

Finally, Fig. 8d shows $P_{ad} - V_l$ diagrams at selected R_l from the NIFTE-NTP and comparison with data taken from Ref. [5] (Fig. 4.23 on p. 162). The two cycles from the NIFTE-NTP were generated with all system parameters set to their nominal (Set-II) values, a nonlinear gain that matches the known temperature difference used in these experiments of $\Delta T_{hx} = 60$ K ($K = 1.02$), and $\mathcal{A} = 330$. As the setting (value) of the feedback resistance

⁵ Based on the total random error of ± 2.5 cm³ for this variable reported in Ref. [5] (on p. 137), and a measured displacement amplitude in the range 10–15 cm³.

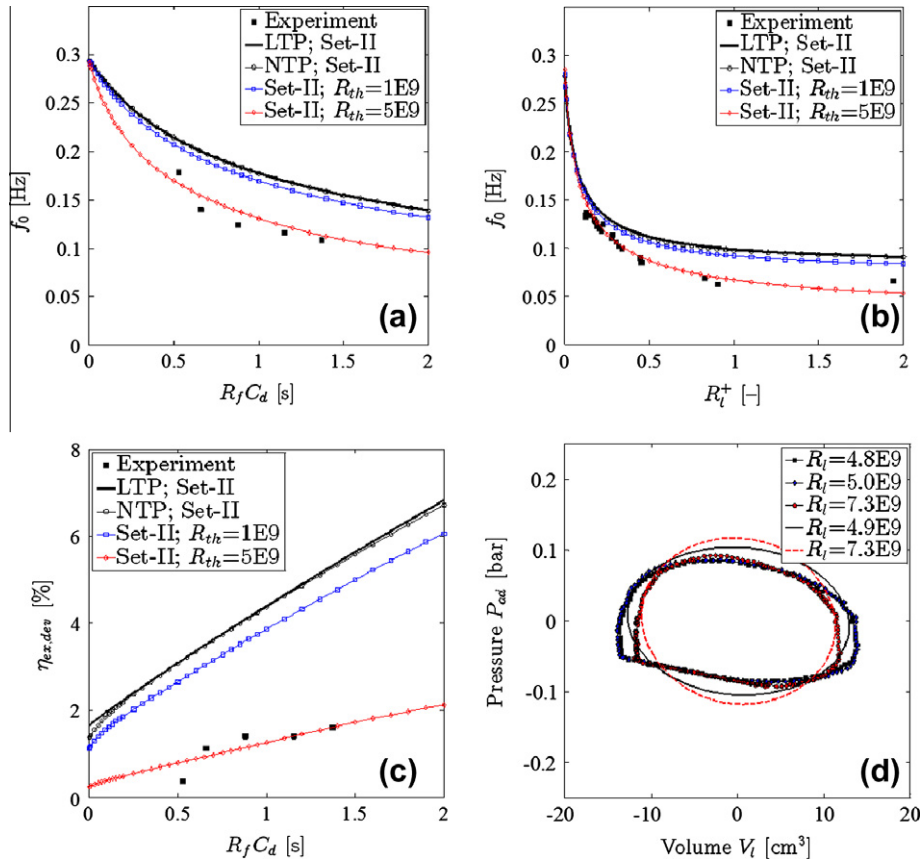


Fig. 8. (a) and (b) Oscillation frequency f_0 for varying $R_f C_d$ and R_l (normalised by its nominal value), respectively. (c) Device exergetic efficiency $\eta_{ex,dev}$ for varying $R_f C_d$. (d) Pressure–volume P_{ad} - V_l diagrams from the NIFTE-NTP model (with a nonlinear gain of $K = 1.02$ corresponding to a HHX-CHX temperature difference of $\Delta T_{hx} = 60$ K) and comparison with experimentally obtained data points taken from Ref. [5] for the range of provided in this reference. Unless otherwise stated, all parameters are set to their Set-II nominal values (stated in Table 3), and $\lambda = 330$.

was not stated, R_f was adjusted to match the measurements. The main experimental observations are captured well; an increase in load resistance R_l leads to reduced liquid displacement amplitudes in the load V_l and (less so) an increased pressurisation of the working fluid in the vapour phase in the adiabatic chamber P_{ad} , though the pressurisation amplitude is slightly overpredicted by the model. The general shapes of these diagrams also reveal information on the phase relationships between the two plotted variables, which on the evidence of Fig. 8d is also well represented by the NIFTE-NTP description.

Thus, it can be concluded that the NIFTE-NTP model can capture the first order effects undergone by the NIFTE device within a range of operation that is close to that corresponding to the experimental prototype pump described in Refs. [3–5], and provide reasonable predictions of its dynamic behaviour and performance. With this in mind it is possible to proceed to a parametric study based on this model, with a view to exploring the NIFTE's design for improved performance.

3.3. Parametric study of operational performance

In a previous study it was observed that the NIFTE is highly sensitive to the capacitance in the power cylinder C_p and the resistance in the feedback tube R_f [6]. In addition to this, the effect of the load parameters, that is the load resistance R_l and inertia L_l , are of great importance to the designer as these are specifications of the device, which are set externally by the application (i.e., the setting within which the NIFTE pump is to operate). The results presented in this section concern the independent perturbation

of each of these parameters within a certain range, while all other parameters are set to their Set-I nominal values. The range over which each parameter is perturbed is given in Table 3. The effects of R_f , R_l , L_l and C_p on the NIFTE's performance are presented in this section. In Fig. 9 and subsequent plots that concern the electrical parameters, the abscissa has been normalised using the nominal value of the corresponding parameter. The nominal value of a parameter is thus observed at a normalised value (denoted by the superscript '+') of $10^0 = 1$.

3.3.1. Condition for oscillation

The minimum value of the gain parameter K necessary for the system to exhibit sustained limit cycle oscillations is given by the critical bifurcation value K^* calculated as the value at which two complex conjugate eigenvalues cross the imaginary axis. The critical value K^* of the gain K allows one to estimate the minimum temperature difference between the heat exchangers that is required to achieve sustained oscillations. In this section, we discuss the effects of the parameters R_f , R_l , L_l and C_p on K^* , i.e., on the minimum temperature difference between the heat exchangers that would be required in order to induce sustained limit cycle oscillations. These four parameters are used throughout the present paper because the NIFTE efficiencies have been shown to be most sensitive to C_p and R_f [6], while the parameters related to the load, R_l and L_l , can reveal important information regarding the most suitable deployment of this early-stage technology.

The plots in Fig. 9 delineate different stability regions. Below these curves the system is (locally) asymptotically stable, whereas above these curves it is unstable. The minimum temperature

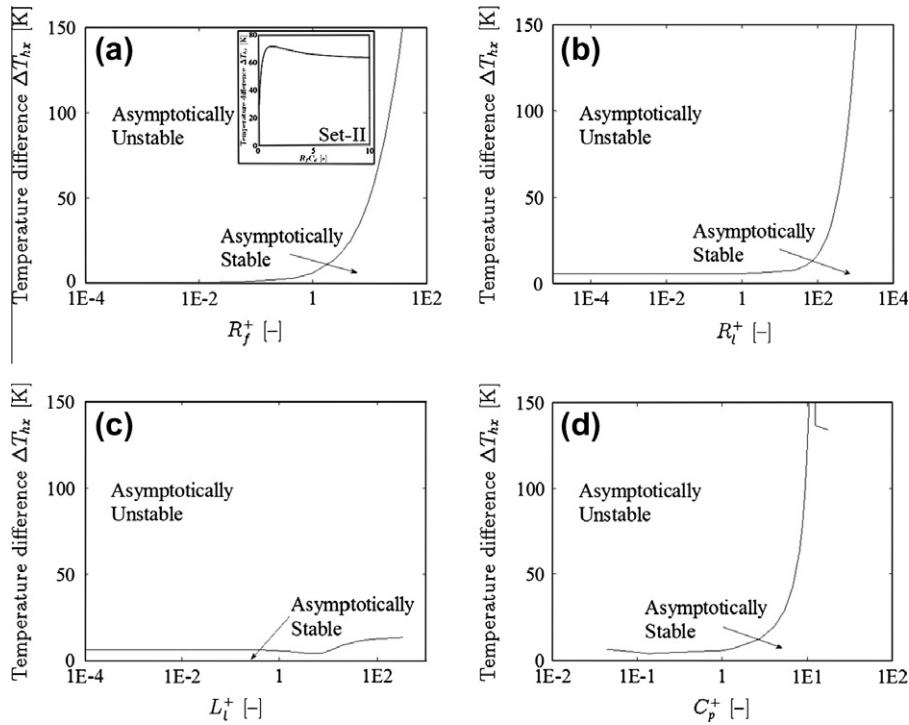


Fig. 9. (a) Temperature difference ΔT_{hx} vs. feedback resistance R_f , (b) temperature difference ΔT_{hx} vs. load resistance R_l , (c) temperature difference ΔT_{hx} vs. inertia in the load L_l , and (d) temperature difference ΔT_{hx} vs. capacitance in the power cylinder C_p . All independent variables are normalised by their respective nominal values (Set-I in Table 3), with the exception of the insert in (a), which shows the Set-II nominal result for ΔT_{hx} as a function of $R_f C_d$, with a nominal C_d .

difference between the HHX and CHX required to make the system unstable for the nominal configuration is approximately 5.7 K, while the minimum temperature gradient at the origin in these conditions is 0.57 K/cm. The value of 5.7 K is about 20 times greater than that predicted by the (linear) Constant Temperature Difference (CTD) model [7,8] for the same (nominal) configuration. On the other hand the temperature gradient is in complete agreement with the value of 0.57 K/cm that was obtained with the NIFTE-LTP model [7]. This is of course expected, as the NIFTE-LTP is a linearised version of the NIFTE-LTP around the equilibrium point. The minimum temperature difference between the heat exchangers increases monotonically as R_f , R_l and C_p increase as shown in Fig. 9a, b and d, respectively. Interestingly, a minimum in the minimum temperature difference required to make the system unstable is observed when perturbing the load inertia L_l , as shown in Fig. 9c.

3.3.2. Oscillation frequency

The effects of the resistance in the feedback tube R_f and the resistance in the load R_l , the inertia in the load L_l and the capacitance in the power cylinder C_p on the oscillation frequency of the NIFTE f_o are shown in Fig. 10. Specifically, Fig. 10a and b shows the frequencies predicted by the NTP and LTP models respectively, when R_f , R_l , L_l and C_p are perturbed within the ranges given in Table 3. The oscillation frequency of the NIFTE is an important performance indicator as it is directly proportional to the pumped hydraulic power and pumped flow-rate capacity of the device.

An important first conclusion is that the frequencies predicted by the LTP and NTP models are almost identical. Experimentally, the NIFTE prototype pump has been reported to operate at $f_o = 0.1\text{--}0.2$ Hz in Refs. [3–5]. Specifically focussing on variations in load and feedback resistance, R_l and R_f , respectively, it was observed that experimentally increasing resistance leads to a lower oscillation frequency [3–5]. From Fig. 10a and b it can be seen that both the LTP and NTP models predict the correct trend for increasing R_f and R_l . So in summary, it can be seen that both the LTP and

the NTP models predict similar frequencies, in broad agreement with actual experimental observations.

Furthermore, in both models, perturbing R_f , R_l and L_l below their nominal respective values does not noticeably affect f_o . On the other hand, the frequency drops monotonically when the same variables are perturbed above their nominal values. The relationship between f_o and C_p shows an interesting feature, which was also reported in Ref. [8]. This involves the appearance of a discontinuity in the oscillation frequency when C_p is perturbed by about 10^1 from its nominal value. It may be concluded that the linear models are perfectly adequate in predicting the oscillation frequency of the NIFTE.

3.3.3. Exergetic efficiency

In order to calculate the device $\eta_{ex,dev}$ and system $\eta_{ex,sys}$ exergetic efficiencies from Eqs. (13a) and (13b) respectively, it was necessary to evaluate the areas enclosed inside the plots of $P_{th}(V_{th})$ in Fig. 7a–c; these plots are equivalent to T – S diagrams, or plots of $T(S)$. To this end, dynamic simulations of the NIFTE-NTP model were run by fixing a value for the gain K that is higher than the critical Hopf bifurcation value K^* . The particular value of K (or, equivalently, temperature difference between the heat exchangers) that was selected is not significant in terms of the resulting efficiency predictions from the model, as long as it is greater than the critical value K^* above which the system exhibits oscillatory, limit cycle behaviour. This statement is made on the evidence of Fig. 6b, which demonstrates that both exergetic efficiencies are almost independent of the value of K . A value of $K = 1.37$, which corresponds to a temperature difference of about 80 K between the heat exchangers that was reported in Ref. [5], was used here to run the dynamic simulations whenever a parameter was perturbed from its nominal value. Recall that in each investigated model configuration (i.e., selection of values for the set of perturbed electrical parameters) in the parametric study, all parameter values other

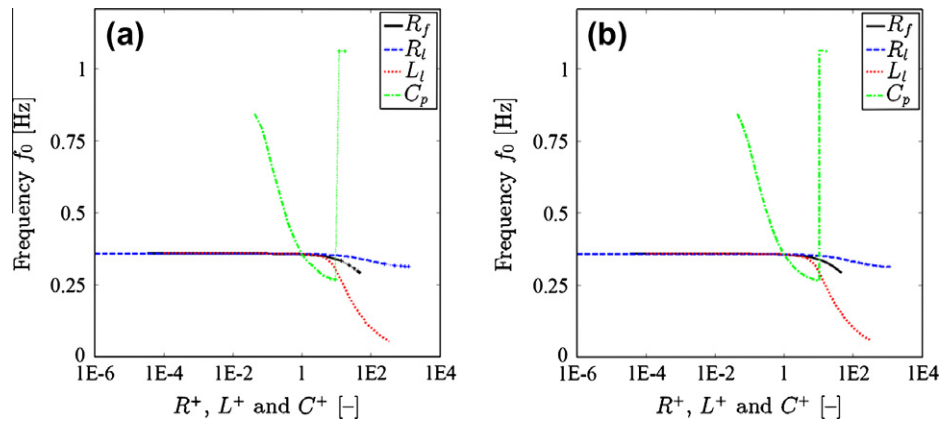


Fig. 10. Effects of the resistance in the feedback tube (R_f), resistance in the load (R_l), inertia in the load (L_l), and capacitance in the power cylinder (C_p) on the oscillation frequency f_0 from the: (a) NIFTE-NTP (nonlinear) model; and (b) NIFTE-LTP (linear) model. The independent variables are normalised by their respective nominal values (Set-I in Table 3). In (a) the nonlinear gain is set to $K = 1.37$ (representing an $\Delta T_{hx} = 80$ °C temperature difference between the heat exchangers), except for the results indicated by the symbols '+' for which the model demonstrated asymptotically stable behaviour (i.e., a lack of oscillation) with $K < K^*$. For these points a higher gain of $K = 3.42$ was used, corresponding to $\Delta T_{hx} = 200$ °C.

than the single one that was being parametrically varied were set to nominal.

However, for some model configurations the Hopf bifurcation point was associated with critical values of nonlinear gain K^* greater than 1.37. Therefore, when investigating the model with these parameter values, using a value of $K = 1.37$ in the dynamic simulations would not have resulted in oscillatory behaviour. To achieve oscillations in this case, values of $K = 3.42$ were employed, representing a temperature difference of 200 K between the heat exchangers. The cases (i.e., model configurations associated with a particular set of parameter values) in which the value for the nonlinear gain used for running dynamic simulation was $K = 3.42$, such that the heat exchanger temperature difference was 200 K, are indicated clearly in these figures by crosses and dashed lines.

Fig. 11 shows results related to the Set-I nominal NIFTE configuration, as described in Table 3 and in Section 2.3.3. The predictions concerning the device exergetic efficiency $\eta_{ex,dev}$ from both the LTP and NTP models indicate that this decreases monotonically as R_f increases, reaching a value of about 1% at the highest investigated values of R_f . Above its nominal value R_f does not affect $\eta_{ex,dev}$ in either model, whereas below its nominal value an increasing R_f causes a decrease in $\eta_{ex,dev}$; this is more evident in the LTP results.

The implication is that the effect of the feedback valve setting on $\eta_{ex,dev}$ is strongly affected by the design of the rest of the NIFTE system; compare for example the trend here with that in Fig. 8c, generate for the Set-II nominal system.

Importantly, although at the lower R_f the linear model (Fig. 11b) tends to predict significantly higher efficiencies, at near-nominal configurations it is associated with lower efficiency values compared to the nonlinear equivalent. In particular with regards to $\eta_{ex,dev}$ at near-nominal values of R_f , the NTP model predicts efficiencies ($\sim 2.5\%$) approximately 2.5 times higher than the equivalent LTP ones ($\sim 1\%$). This arises possibly as a consequence of the difference in the input pressures in the two models. In any case, these values are considered low, but in relatively good agreement with direct experimental evidence [5,6]. For comparison, from Ref. [5], the device exergetic efficiency was stated as being between 0.4% and 1.6% increasing monotonically with increasing R_f .

Further, the system exergetic efficiency $\eta_{ex,sys}$ in the NIFTE prototype was measured and found to be between 3% and 10% [5]. It can be seen in Fig. 11 that, unlike the device efficiency, $\eta_{ex,sys}$ does not increase monotonically with decreasing R_f . The NTP model reveals an optimum value at low resistance settings, whereas the LTP model shows a continual improvement as R_f is progressively reduced. Both models predict the efficiencies in the correct range

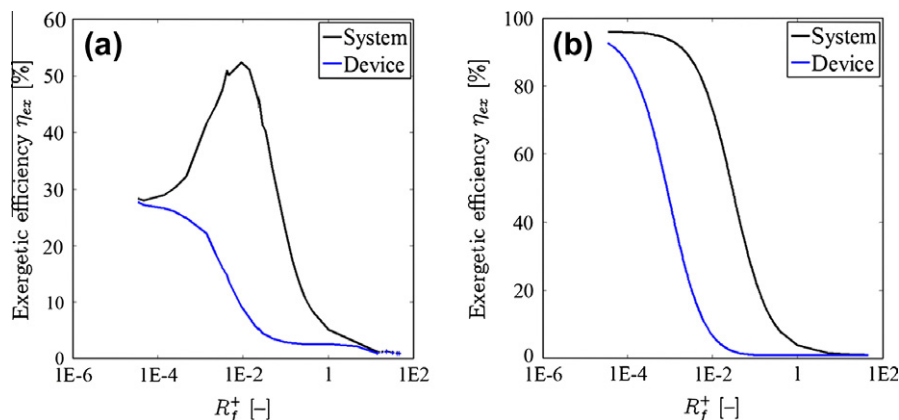


Fig. 11. Effect of the feedback resistance R_f on the two measures of the NIFTE exergetic efficiency η_{ex} from the: (a) NIFTE-NTP (nonlinear) model; and (b) NIFTE-LTP (linear) model. R_f is normalised by its nominal value (Set-I in Table 3). In (a) the nonlinear gain is set to $K = 1.37$ (representing an $\Delta T_{hx} = 80$ °C temperature difference between the heat exchangers), except for the results indicated by the symbols '+' for which the model demonstrated asymptotically stable behaviour (i.e., a lack of oscillation) with $K < K^*$. For these points a higher gain of $K = 3.42$ was used, corresponding to $\Delta T_{hx} = 200$ °C.

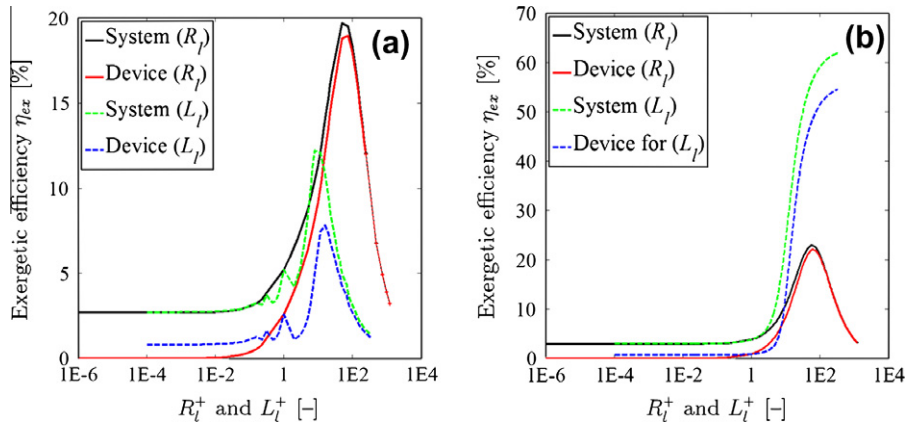


Fig. 12. Effect of the load resistance R_l and load inertia L_l on the two measures of the NIFTE exergetic efficiency η_{ex} from the: (a) NIFTE-NTP (nonlinear) model; and (b) NIFTE-LTP (linear) model. The load variables are normalised by their respective nominal values (Set-I in Table 3). In (a) the nonlinear gain is set to $K = 1.37$ (representing an $\Delta T_{hx} = 80$ °C temperature difference between the heat exchangers), except for the results indicated by the symbols '+' for which the model demonstrated asymptotically stable behaviour (i.e., a lack of oscillation) with $K < K^*$. For these points a higher gain of $K = 3.42$ was used, corresponding to $\Delta T_{hx} = 200$ °C.

and order of magnitude. When R_f is increased by a factor of more than 10^2 relative to its nominal value, the device and system exergetic efficiencies deteriorate and approach each other to a value of about 1%, in both models.

Results related to variations in the load (R_l and L_l) beyond the nominal configuration explored above are shown in Fig. 12. The device and system exergetic efficiencies show a peak in the nonlinear model when both R_l and L_l (Fig. 12a) are perturbed past the nominal values. This finding has noteworthy implications for the design of these devices. Furthermore, the linear model predicts maximum efficiencies of about 60% for the range of R_l and L_l investigated, whereas the nonlinear model predicts maximum efficiencies of about 20%. This may be explained by the fact that, unlike the linear model, the nonlinear model does not allow temperature excursions outside the saturation temperature amplitude in the heat exchanger walls as the liquid level in the displacer cylinder approaches the ends of the heat exchangers. The 60% prediction for the efficiencies from the linear model is unrealistically high; the maximum system exergetic efficiency observed experimentally was reported as $\sim 10\%$ [5]. It is also evident from these figures that the nominal configuration is acutely sub-optimal, with significantly lower efficiencies than the maximum values reported here.

Lastly, the effect of the capacitance in the cylinder C_p on the exergetic efficiency measures is shown in Fig. 13. The discontinuity

that appears in the exergetic efficiency that has been previously presented in the LTP model [8] is also observed in the NTP model when perturbing C_p , so this is not a result of the nonlinearity, but of the switch in the dominant frequency in the output of the system reported in Ref. [8]. Both the LTP and NTP models predict high efficiencies, with the LTP model predicting generally higher values, as before, especially at low values of C_p . The discontinuity at higher C_p has not been reported experimentally, but this is due to the fact that such high values of C_p have not been previously employed. It is something that is worth attempting in future investigations.

4. Further discussion and conclusions

A nonlinearity has been introduced into an existing (linear) model for the NIFTE fluid pump, whereby the temperature of the heat exchangers is allowed to saturate at long distances from the equilibrium level that is found halfway between the two heat exchanger blocks. Simulations with this model have shown that its frequency of oscillation does not depend on the temperature difference between the hot and the cold heat exchangers, and also, that this frequency is similar to that predicted by the previous linear models [6–9] and is in reasonable agreement with experiments on a NIFTE prototype [3–5]. It was also found that the predicted exergetic efficiency of the model for this device does not depend

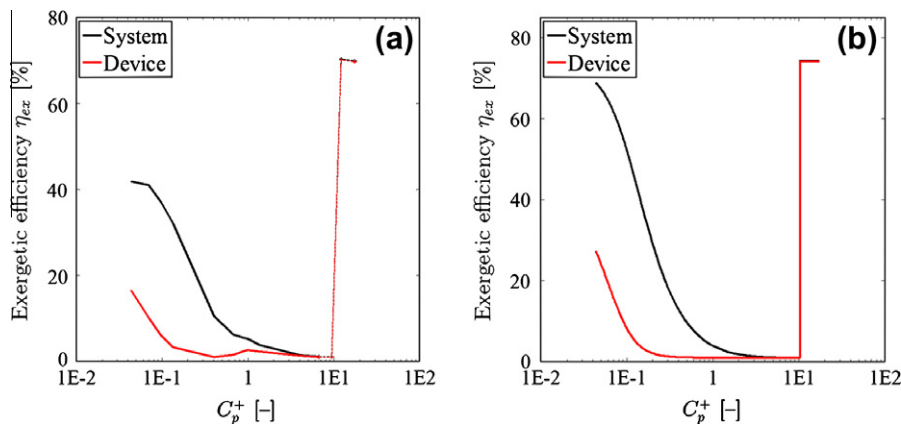


Fig. 13. Effect of the power cylinder capacitance C_p on the two measures of the NIFTE exergetic efficiency from the: (a) NIFTE-NTP (nonlinear) model; and (b) NIFTE-LTP (linear) model. C_p is normalised by its nominal value (Set-I in Table 3). In (a) the nonlinear gain is set to $K = 1.37$ (representing an $\Delta T_{hx} = 80$ °C temperature difference between the heat exchangers), except for the results indicated by the symbols '+' for which the model demonstrated asymptotically stable behaviour (i.e., a lack of oscillation) with $K < K^*$. For these points a higher gain of $K = 3.42$ was used, corresponding to $\Delta T_{hx} = 200$ °C.

on the temperature difference between two heat exchangers when heat at up to ~ 300 °C is used.

Parameters that have been previously observed to influence strongly the behaviour of the NIFTE [6] were perturbed from their nominal values (associated with the reported experimental prototype) and comparison was made with observations from the linear models. Parameters that are related to the load (the liquid flow resistance and inertia) were also perturbed since it is believed that they can reveal important information regarding the practical employment of the technology. Both linear and nonlinear models predict similar trends for the oscillation frequencies as a function of the investigated parameters. Values of these parameters in the load and in the feedback connection that are higher than the nominal ones lead to a decrease in the oscillation frequency, while the trend of frequency as a function of the capacitance of the adiabatic volume shows a minimum at values greater than nominal.

The linear model typically predicts higher exergetic efficiencies than the nonlinear equivalent, and outside the range that has been reported experimentally. This can be explained by the fact the LTP model does not consider the saturation in the temperature of the heat exchanger walls as the liquid level in the displacer cylinder covers an ever increasing extent (overlap) of the heat exchangers. The NIFTE is shown to be most efficient at low values of feedback resistance, and with an optimal load that has a higher resistance and inductance (i.e., higher liquid flow drag and inertia) than that used in the nominal prototype configuration. Furthermore, a strong discontinuity arises when the capacitance of the adiabatic volume (i.e., the ratio of the time-averaged volume to the time-averaged pressure of the combined vapour volume at the top of the engine) is perturbed above a certain value. This discontinuity was also observed in the linear models, and in agreement with those related studies, operation at capacitance values beyond this discontinuity results in greatly improved efficiencies. The capacitance value at which this is observed is also greater than that used in the nominal prototype.

Lastly, a numerical simulation of the nonlinear NIFTE model was performed in conditions representative of operation with low-grade heat. The results indicate that the frequency of oscillations is independent of the temperature difference between the heat exchangers, while the amplitude is a strong function of this temperature difference. This is a noteworthy finding. One can conclude that it is possible control the amplitude of the limit cycle oscillations (and hence, the pumping capacity) of the device independently of its frequency by varying the temperature difference between the heat exchangers. The relationship between the temperature difference and the frequency of the limit cycle oscillation, as well as the identification of the parameter that can allow us to control the frequency independently of the amplitude of oscillation provides us with valuable information for the design of more efficient NIFTE and will be an excellent starting point for future studies and implementations.

Appendix A. Estimation of NTP model parameter β

Let the vertical temperature profile on the surfaces of the NIFTE heat exchangers be given by,

$$T_{hx} = \alpha \tanh(\beta z) \quad (\text{A.1})$$

Clearly, α is the *maximum available* temperature amplitude in the heat exchangers, or half of the maximum available temperature difference between the hot and cold heat exchangers $\Delta T_{hx} = \max\{T_{hx}\} - \min\{T_{hx}\}$, and the product $\alpha\beta$ is equal to the spatial gradient of the temperature profile in the heat exchangers $T_{hx}(z)$ at (and near) the equilibrium at $z = 0$, such that the gradient depends on both parameters α and β . In this study α is a variable

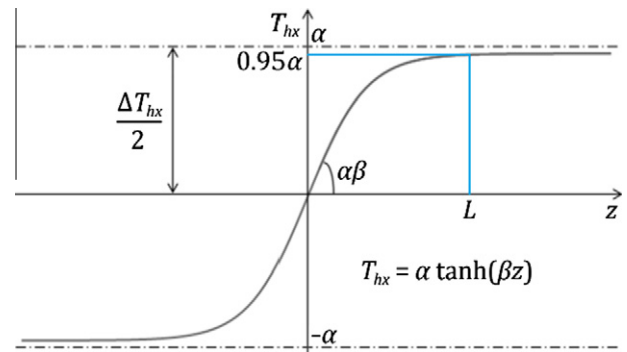


Fig. A.1. Heat exchanger wall temperature against height in the heat exchangers (relative to the equilibrium temperature T_0); showing the definition of parameter β from the condition $T_{hx} = 0.95\alpha$.

and is related to the nonlinear gain K (see Eq. (9)), whereas a value for β is required in order to solve the system of equations for the NIFTE-NTP.

The term βy in the bracket in Eq. (A.1) is dimensionless. This implies that β must be of dimension L^{-1} , and therefore we can say that β scales with the inverse of the total height L of the heat exchanger block. Substituting for $\alpha = \Delta T_{hx}/2$ in Eq. (A.1), we obtain an expression for β ,

$$\beta = \frac{1}{L} \tanh^{-1} \left(\frac{T_{hx}}{\Delta T_{hx}/2} \right). \quad (\text{A.2})$$

The factor of 2 in Eq. (A.2) comes from the fact that the amplitude in T_w is being compared to *half* of the temperature difference between the heat exchangers, as indicated in Fig. A1.

A value of β was calculated by requiring the temperature profile in the heat exchangers to achieve 95% saturation of ΔT_{hx} (i.e., $T_{hx}/\alpha = T_{hx}/(\Delta T_{hx}/2) = 0.95$) when $z = L = 0.09$ m, which was the length of the HHX block stated in Ref. [5]. This value of β also sets the increase of T_{hx} relative to its value at $z = 0$ to ~ 15 – 20% of α in the first 10%, ~ 30 – 40% of α in the first 20%, and $\sim 50\%$ of α in the first 30% of the HHX height L . This spatial temperature profile rise is consistent with: (i) approximate heat transfer scaling arguments; (ii) a simplified numerical simulation of the unsteady heat transfer in the HHX block; and (iii) the reported geometry and conditions in the NIFTE prototype heat exchangers [5] and visual observations of the NIFTE device in operation [23], all based on 125–150 W of electrical heating leading to $\alpha = \Delta T_{hx}/2 = 30$ – 50 K [3–5]. This choice gives $\tanh^{-1}(0.95) = 1.8$, and therefore, $\beta = 20$ m^{-1} from Eq. (A.2). The choice is demonstrated in Fig. A1, which shows a plot of the vertical temperature profile in the heat exchangers that reaches 95% of the saturation value attained by $z = L = 0.09$ m. This value of β was used for all runs contained in the present paper.

References

- [1] Markides CN. The role of pumped and waste heat technologies in a high-efficiency sustainable energy future for the UK. Appl Therm Eng, in press.
- [2] Crook AW. Profiting from low-grade heat: thermodynamic cycles for low-temperature heat sources. London: The Institution of Electrical Engineers; 1994.
- [3] Smith TCB. Power dense thermofluidic oscillators for high load applications. AIAA-2004-5758. In: Energy conversion engineering, IECEC 2004: Proceedings of the 2nd international energy conversion engineering conference; 2004 August 16–19; Providence (RI), USA. Reston (VA): AIAA; 2004. p. 1–15.
- [4] Smith TCB. Asymmetric heat transfer in vapour cycle liquid-piston engines. In: Stirling engine, ISEC 2005: proceedings of the 12th international Stirling engine conference and technology exhibition; 2005 September 7–9; Durham, UK. Durham: Durham University; 2005. p. 302–14.
- [5] Smith TCB. Thermally driven oscillations in dynamic applications. PhD thesis. Cambridge: University of Cambridge, UK; 2006.
- [6] Markides CN, Smith TCB. A dynamic model for the efficiency optimization of an oscillatory low-grade heat engine. Energy 2011;36:6967–80.

- [7] Solanki R, Galindo A, Markides CN. Dynamic modelling of a two-phase thermofluidic oscillator for efficient low-grade heat utilization: effect of fluid inertia. *J Appl Energy* 2012;89:165–263.
- [8] Solanki R, Galindo A, Markides CN. The role of heat exchange on the behaviour of a two-phase thermofluidic oscillator. *Appl Therm Eng*, in press.
- [9] Solanki R, Mathie R, Galindo A, Markides CN. Irreversible thermal losses in a two-phase thermofluidic oscillator. *J Appl Energy*, accepted for publication.
- [10] Backhaus S, Swift GW. A thermoacoustic-stirling heat engine: detailed study. *J Acoust Soc Am* 2000;107:3148–66.
- [11] Ceperley PH. A pistonless stirling engine—the traveling wave heat engine. *J Acoust Soc Am* 1979;66:1508–13.
- [12] Huang BJ, Chuang MD. System design of orifice pulse-tube refrigerator using linear flow network analysis. *Cryogenics* 1996;36:889–902.
- [13] Daw CS, Kennel MB, Finney CEA, Connolly FT. Observing and modeling nonlinear dynamics in an internal combustion engine. *Phys Rev E* 1998;57:2811–9.
- [14] Chen L, Sun F, Wu C. Influence of heat transfer law on the performance of a Carnot engine. *Appl Therm Eng* 1997;17:277–82.
- [15] Hoffmann KH, Burzler JM, Schubert S. Endoreversible thermodynamics. *J Non-Equilib Thermodyn* 1997;22:311–55.
- [16] Sun F, Chen W, Chen L, Wu C. Optimal performance of an endoreversible Carnot heat pump. *Energy Convers Mgmt* 1997;38:1439–43.
- [17] Martinez-Martin T. State-space formulation for circuit analysis. *IEEE Trans Educ* 2010;53(3):497–503.
- [18] Dorf RC, Bishop RH. *Modern control systems*. London: Prentice Hall; 2010.
- [19] Strogatz SH. *Nonlinear dynamics and chaos: with applications to physics, biology, chemistry and engineering*. Cambridge: Westview Press; 2000.
- [20] Dhooge A, Govaerts W, Kuznetsov YA, Mestrom W, Riet AM, Sautois B. MATCONT and CL_MATCONT: continuation toolboxes in MATLAB, online manual; December 2006. <http://www.ricam.oeaw.ac.at/people/page/jameslu/Teaching/LectureNotes/II_Lecture2/manual.pdf> [accessed 07.01.12].
- [21] Dormand JR, Prince PJ. A family of embedded Runge–Kutta formulae. *J Comput Appl Math* 1980;6:19–26.
- [22] Smith JM, Van Ness HC, Abbott MM. *Introduction to chemical engineering thermodynamics*. 6th ed. London: McGraw-Hill; 2001.
- [23] Thermofluidics. NIFTEPumpDemo.mov, online video; uploaded 9 June, 2010. <<http://youtu.be/mi7xO-PQtEU>> [accessed 17.02.12].